The cerebellum is involved in processing of predictions and prediction errors in a fear conditioning paradigm

Ernst TM[1,2], Brol A[1], Gratz M[2,3], Ritter C[1], Bingel U[1], Schlamann M[4,5], Maderwald S[2], Quick HH[2,3], Merz CJ[6]*, Timmann D[1,2]*

* shared senior authorship

Affiliations:

[1] Department of Neurology, Essen University Hospital, Essen, Germany

[2] Erwin L. Hahn Institute for Magnetic Resonance Imaging, University of Duisburg-Essen, Essen, Germany

[3] High-Field and Hybrid MR Imaging, Essen University Hospital, Essen, Germany

[4] Institute of Diagnostic and Interventional Radiology and Neuroradiology, Essen University Hospital, Essen, Germany

[5] Department of Neuroradiology, University Hospital Cologne, Cologne, Germany

[6] Institute of Cognitive Neuroscience, Department of Cognitive Psychology, Ruhr University Bochum, Bochum, Germany

Corresponding author:

Ernst, Thomas M.

Essen University Hospital, Dept. of Neurology

Hufelandstr. 55, 45147 Essen, Germany

Email: thomas.ernst@uk-essen.de

Phone +49 201 723 2594, Fax +49 201 723 5969

Running title: Cerebellum and fear conditioning

Keywords: Emotions; extinction; fear; vermis; cerebellar hemisphere; aversive conditioning

Acknowledgments: Funded by the Deutsche Forschungsgemeinschaft (DFG, German Research Foundation) – project number 316803389, SFB 1280, subprojects A05, A09, and A11

Abstract

Prediction errors are thought to drive associative fear learning. Surprisingly little is known about the possible contribution of the cerebellum. To address this question, healthy participants underwent a differential fear conditioning paradigm during 7T magnetic resonance imaging. An event-related design allowed us to separate cerebellar fMRI signals related to the visual conditioned stimulus (CS) from signals related to the subsequent unconditioned stimulus (US; an aversive electric shock). We found significant activation of cerebellar lobules Crus I and VI bilaterally related to the CS+ compared to the CS-. Most importantly, significant activation of lobules Crus I and VI was also present during the unexpected omission of the US in unreinforced CS+ acquisition trials. This activation disappeared during extinction when US omission became expected. These findings provide evidence that the cerebellum has to be added to the neural network processing predictions and prediction errors in the emotional domain.

Introduction

Cerebellar disease has long been known to result in disordered motor performance and motor learning (Holmes, 1908; McCormick and Thompson, 1984). Evidence has accumulated that cerebellar patients also present with various degrees of cognitive, emotional and behavioral abnormalities (Schmahmann and Sherman, 1998). Because the microscopic structure of the cerebellum is highly homogeneous, it is often assumed that the cerebellum performs one single neural operation (Caligiore et al., 2017; Miall and Galea, 2016; Popa et al., 2014; Sokolov et al., 2017). The most popular current hypothesis states that the cerebellum acts as or is part of a predictive device (Popa and Ebner, 2018 for recent review). In the motor domain, it is assumed that the cerebellum is crucially involved in the prediction of the sensory consequences of motor commands thought to be achieved via internal models (Bastian, 2006; Miall et al., 1993; Wolpert et al., 1998). These internal models have to be constantly adapted due to a constantly changing inner and outer environment. Assumedly, the difference between the predicted and actual sensory outcome results in a sensory prediction error used to adapt the internal model and subsequent motor behavior. Although most studies have been performed in the motor domain, there is initial evidence that the cerebellum is involved in predictive control in the cognitive domain (Lesage et al., 2012; Lesage et al., 2017; Moberget et al., 2014). The aim of the present study was to show that this assumption also applies to the emotional domain.

Fear conditioning was used as a model system because the cerebellum is involved in the acquisition of learned fear responses (Lange et al., 2015; Maschke et al., 2002; Ploghaus et al., 1999; Sacchetti et al., 2002), and has known connections with several parts of the neural network underlying fear conditioning, including the limbic system (Badura et al., 2018; Blatt et al., 2013). Furthermore, prediction errors are thought to be the main drivers of associative fear learning (Holland and Schiffino, 2016; Rescorla and Wagner, 1972). In the fear conditioning literature, however, the possible role of the cerebellum in aversive prediction error processing has largely been ignored (Apps and Strata, 2015; Tovote et al., 2015). Previous studies focused on the role of the amygdala, insula, midbrain periaqueductal gray and striatum (Boll et al., 2013; Li et al., 2011; Li and McNally, 2014). We wanted to provide

initial evidence that the cerebellum has to be added to the neural network processing predictions errors in learned fear responses.

During fear conditioning, participants learn to predict that the initially neutral conditioned stimulus (CS) is followed by an unpleasant unconditioned stimulus (US). As a result, fear responses are elicited already at the time of CS presentation. The initial occurrence of the US is unexpected and has been considered as an error signal (Taylor and Ivry, 2014). An event-related functional magnetic resonance imaging (fMRI) design allowed us to separate blood oxygenation level dependent fMRI signals related to the CS from signals related to the subsequent US. Participants learn within a very limited number of trials that the CS predicts the occurrence of the US, particularly if appropriate instructions are provided (Atlas et al., 2016; Tabbert et al., 2011). In case the cerebellum is involved in prediction of the US, cerebellar fMRI signals should be high during CS presentation. As soon as learning has occurred, the occurrence of the US is expected. Thus, if the hypothesis is correct that the cerebellum contributes to aversive prediction errors, cerebellar activation should be increased at the time of the unexpected omission of the US (due to a partial reinforcement schedule). During extinction, that is the repeated presentation of CS-only trials, the omission of the US becomes expected and cerebellar fMRI signals at the time of the US omission should decrease.

In accordance with the fMRI literature (Lange et al., 2015), we found cerebellar activations related to the prediction of the US. In addition, marked cerebellar activation was present during the unexpected omission of the US, which disappeared during extinction. Our findings are consistent with the hypothesis that the cerebellum is involved in the processing of aversive predictions and prediction errors and has to be added to the neural network underlying emotional associative learning.

98 # Materials and Methods

99 ## Participants

100 Experiment power was estimated based on previous eyeblink conditioning data, which had
101 also been acquired at 7 T (Ernst et al., 2017) using the fmripower toolbox for MATLAB
102 (fmripower.org; Mumford, 2012). Considering CS-only trials in acquisition and aiming for a
103 power of 80 % at $p < 0.001$, group sizes were estimated to 21 participants for lobule VI
104 ipsilaterally to US application.

105 A total of 27 young and healthy participants performed the experiment. Three participants
106 had to be excluded due to technical errors, one participant due to an incidental finding on
107 brain MRI, and one participant due to constant motion throughout MRI acquisition. Thus, a
108 total of 22 participants (8 males, 14 females, mean age: 26.9 (SD = 4.3) years, range: 19 to
109 32 years) were included in the final data analysis. None of the participants presented with
110 neurological or neuropsychiatric disorders based on medical history. None were taking
111 centrally-acting drugs, except two who were taking a low dosage of a corticosteroid and an
112 antihistamine, respectively. All participants were right-handed based on the Edinburgh
113 handedness inventory (Oldfield, 1971) and had normal or corrected-to-normal vision. They
114 were asked to refrain from alcohol consumption the night before the experiment. Informed
115 consent was obtained from all participants. The study was approved by the local ethics
116 committee and conducted in accordance with the Declaration of Helsinki.

117 ## Fear conditioning

118 The entire experiment was performed within one session inside the MRI scanner. The
119 paradigm presentation was controlled by a computer running the software Presentation
120 (version 16.4, Neurobehavioral System Inc., Berkeley, CA). **Figure (Fig.) 1** displays the
121 experimental paradigm. Participants were shown images of the visual stimuli used in the
122 experiment and told that electrical shocks would be applied during the experiment. They
123 were instructed that, should they perceive a pattern between CS and US presentations, the
124 experimenter would not change it during the experiment.

125

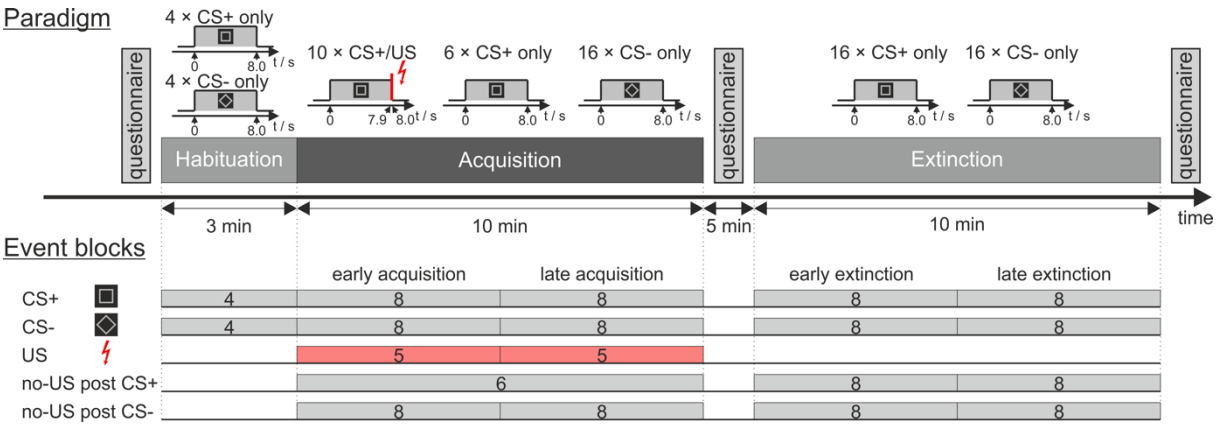

Figure 1: Experimental paradigm and overview of individual events. CS = conditioned stimulus; US = unconditioned stimulus. For further details see text.

Visual stimuli were projected onto a rear projection screen inside the scanner bore using a standard projector. Images were visible to the participants through a mirror mounted on the radiofrequency (RF) head coil. Two pictures of black-and-white geometric figures (a square and a diamond shape, i.e. the square tilted by 45°) of identical brightness were used as CS+ and CS- (time of presentation: eight seconds). In reinforced CS+ trials (i.e. 10 out of 16 acquisition trials), the visual stimulus co-terminated with the presentation of the aversive US. In CS- trials, the visual stimulus was never followed by the aversive US. A neutral black background image was displayed in between visual stimulus presentations (ITI randomized between 16 s and 20 s). Use of the two figures as CS+ and CS- was pseudo-randomly counterbalanced between the individual participants.

A short electrical stimulation was used as an aversive US. The electrical stimulation was generated by a constant current stimulator (DS7A, Digitimer Ltd., London, UK) and applied to the left hand via a concentric (ring-shaped) bipolar surface electrode with 6 mm conductive diameter and a central platinum pin (WASP electrode, Specialty Developments, Bexley, UK). For MR-safety reasons, an in-house build non-magnetic high-resistivity electrode lead was used to connect the stimulator with the surface electrode (Schmidt et al., 2016). The 100 ms US consisted of a short train of four consecutive 500 µs current pulses (maximum output voltage: 400 V) with an inter pulse interval of 33 ms. Immediately before start of MRI measurements, stimulation current was gradually increased, and participants were asked to report on the perceived sensation intensity until an “unpleasant but not painful” intensity

was reached (mean current: 3.9 (SD = 2.3) mA, range 1.6 to 9.3 mA). The final individual current setting was kept constant for all stimulations. Stimulus timing was set for the US to co-terminate with visual CS+ presentation.

During the experiment three types of trials were presented to the participants: CS+ followed by an US (paired CS+/US trial), CS+ without an US (CS+ only trial) and CS- without US (CS- only trial). The experimental protocol consisted of the three phases: "habituation" (4 CS+ only trials, 4 CS- only trials, presented in alternating order), "acquisition" (10 paired CS+/US trials, 6 CS+ only trials, 16 CS- only trials) and "extinction" (16 CS+ trials, 16 CS- only trials). Different trials types in acquisition and extinction were presented in a pseudorandomized order with four restrictions: Firstly, the first two trials of acquisition were set to be paired CS+/US trials, secondly, there were never more than two consecutive CS of one kind presented in a row, thirdly, during acquisition and extinction the number of events of each kind was kept identical in the first half and in the second half of the experiment, and fourthly, the very last trial of acquisition was set to be a paired CS+/US trial. During acquisition, the order of events was the same for all participants, while use of the two different figures as CS+ and CS- was counterbalanced across the whole group. Order of CS+ and CS- events was counterbalanced during extinction (12 starting with CS+, 10 starting with CS-), and habituation (15 starting with CS+, 7 starting with CS-). Each experimental phase was performed within a separate block of fMRI data acquisition.

Questionnaires

Participants were required to answer three questionnaires, one before the start of the experiment, a second one in between acquisition phase and extinction phase and a third questionnaire after the experiment. The first and the third questionnaires were print copies handed out to the participant. The second questionnaire was projected onto the screen inside the MRI scanner bore one question at a time and answers were given orally via an intercom system.

Participants were asked to rate their (hedonic) valence and (emotional) arousal on viewing images of the CS+ and CS- on a nine-step Likert scale from "very unpleasant" to "very pleasant" and "quiet and relaxed" to "very excited", respectively. Additionally, the questionnaire following acquisition contained five questions regarding US perception and

CS-US contingency: rating of the last US on a nine step-scale ("not unpleasant" to "very unpleasant"); a multiple-choice question and an percentage estimate whether the US was applied after the presentation of the square and the diamond shaped CS (options: "always", "sometimes", "never", "I cannot answer"); and lastly an estimation after which time and number of US presentations, if at all, a connection between the visual stimuli and the US presentation was identified.

Statistical analyses were performed using SPSS software (Version 24, IBM Corp., Armonk, NY). Using repeated measure analyses of variance (ANOVA) valence and arousal ratings were tested for within subject effects of stimulus type (CS+ vs. CS-) and phase (pre-acquisition, post-acquisition vs. post-extinction). Where necessary individual ratings were compared with post-hoc *t*-tests.

Physiological data acquisition

Physiological data measured throughout the experiment were skin conductance response (SCR), pulse rate and breathing rate. Skin conductance (SC) was acquired using a physiological data acquisition station with a dedicated MRI-compatible SC module and appropriate hardware filters sampling at 2 kHz (EDA 100C-MRI, BIOPAC Systems Inc., Goleta, CA). SC electrodes were attached to the participants' left middle and ring fingers.

Pulse rate and breathing rate were measured using the physiologic monitoring unit (PMU) provided by the MRI scanner (Siemens Healthcare GmbH, Erlangen, Germany). In detail, pulse oximetry signals were recorded using a wireless recording device clipped to the participant’s right index finger. A respiratory bellows was attached to the participant's lower abdomen using a hook-and-loop belt.

Skin conductance analysis

To eliminate high-frequency noise and low-frequency drifts SC data was bandpass filtered (-61 dB Blackman FIR filter, 0.5 to 10 Hz) using AcqKnowledge software (BIOPAC Systems Inc., Goleta, CA). All further SC data processing was performed using MATLAB software (Release 2017a, The MathWorks Inc., Natick, MA). Semi-automated peak detection was performed, and SCR were defined as the maximum trough-to-peak-amplitude of any SCR peak within a given time interval. In each trial, SCR were evaluated for three distinct time windows (Prokasy and Ebel, 1967): the first interval response (FIR) within a time window of

1.0 s to 5.0 s after CS onset, the second interval response (SIR) within a time window of 5.0 s to 8.5 s after CS onset, and the unconditioned response window (i.e. third interval response, TIR) 8.5 s to 13.0 s after CS onset (irrespective whether a US was presented in the particular trial or not) (**Fig. 2b**). To normalize data SCR values were increased by 1 µS and logarithmized (Boucsein, 2012; Venables and Christie, 1980). Mean SCR values were calculated grouped for blocks of five, six and eight events, corresponding to the first-level regressor selection in MRI analysis.

Statistical analyses were performed using SPSS software (Version 24, IBM Corp., Armonk, NY). ANOVA with repeated measures were calculated for within subject effects of stimulus type (CS+ vs. CS-) and block (early vs. late) considering SCR values as dependent measure. Appropriate post-hoc *t*-tests were calculated. Because there was only one block of unpaired CS+ trials in acquisition (see **Fig. 1**), differences of TIR in unpaired CS+ trials with TIR in paired CS+ and CS- trials were analyzed using *t*-tests.

MRI acquisition

All MR images were acquired with the participants lying supine inside a whole-body MRI system operating at 7 Tesla magnetic field strength (MAGNETOM 7T, Siemens Healthcare GmbH, Erlangen, Germany) equipped with a 1-channel transmit / 32-channel receive RF head coil (Nova Medical, Wilmington, MA). To homogenize the RF excitation field (B1), three dielectric pads filled with high-permittivity fluid were placed below and on either side of each participants' upper neck (Teeuwisse et al., 2012). As needed, further cushions were used to fix the head position within the RF coil.

Prior to fMRI acquisition a sagittal MP2RAGE sequence (Gallichan and Marques, 2017; Marques et al., 2010) was run to acquire whole-brain anatomical reference images with an isotropic voxel size of 0.75 mm. Further imaging parameters were set as follows: TR/TE, 6000/3.45 ms, TI1/TI2, 800/2700 ms, flip angles 1/2, 4°/5°, parallel acceleration factor, 3, phase and slice partial Fourier factor, 6/8, acquisition matrix, 320 × 300, number of slices, 192, TA, 9:40 min.

Whole brain functional fMRI acquisition was performed using a fat-saturated, two-dimensional simultaneous multi slice echo planar image (SMS-EPI) sequence (Cauley et al., 2014; Setsompop et al., 2012) with an isotropic voxel size of 1.7 mm, in three consecutive

episodes for habituation (90 volumes), acquisition and extinction (320 volumes each). Imaging parameters were selected as follows: TR/TE, 2000/22 ms, flip angle, 70°, parallel acceleration factor, 2, SMS factor, 3, phase partial Fourier factor, 6/8, acquisition matrix, 130 × 130, number of slices, 90.

Image processing

All image and fMRI analyses were performed using SPM 12 (Wellcome Department of Cognitive Neurology, London, UK) on a platform running MATLAB on Mac OS X 10.12.6, if not explicitly stated otherwise. SPM default brightness threshold was set from 0.8 to 0.1 to avoid signal dropouts within the hypointense cerebellar nuclei (Thürling et al., 2015).

Brain extraction was performed on non-denoised uniform T1 weighted (UNI) volumes using the CBS tools for high-resolution processing of high-field brain MRI (Bazin et al., 2014). Best coregistration of the mean functional volume to the brain extracted structural volume was achieved by using the function "epi_reg" available in FSL (Release 5.0.10, Centre for Functional MRI of the Brain, Oxford, UK).

Normalization of the cerebellum was performed using the SUIT-toolbox for SPM (version 3.1). Using the spatially unbiased atlas template of the human cerebellum (SUIT, Diedrichsen, 2006) brain-extracted structural volumes were segmented, and cerebellar masks were generated. Manual correction of each mask was performed by an experienced technician using MRIcron software (Rorden and Brett, 2000). The segmented structural images and the cortical cerebellar mask were supplied to a ROI-based DARTEL normalization algorithm available within the SUIT toolbox, and a cerebellar normalization was calculated. In addition, whole-brain normalization to MNI-space was obtained using the SPM segment routine.

Functional MRI volumes for each participant were corrected for slice timing and realigned to the first volume of the habituation phase. Functional volumes were then separately normalized to SUIT space (cerebellum only) and MNI space (whole brain), and smoothed by an isotropic smoothing kernel of 4 mm.

fMRI analysis

We focused our fMRI analysis on the cerebellum. In addition, exploratory analysis of the whole brain was performed. The first-level analysis was modelled as an event related-design

(durations set to 0 s). The first five volumes of each fMRI run were disregarded. Events were blocked into 19 regressors of interest as displayed in **Fig. 1**. If number of trials allowed ($n \geq 4$), events of each kind were grouped in two equal-sized blocks representing the first (early) and the second (late) half of each phase. Regressors were chosen for CS+ and CS- during habituation (2 regressors, 4 events each), CS+ and CS- presentations during acquisition and extinction (8 regressors, 8 events each), US presentations during acquisition (2 regressors, 5 events each), and the omission of US presentations (no-US) at the expected time of US presentations after CS onset (no-US post CS+: 1 regressor, 6 events during acquisition, 2 regressors, 8 events each during extinction; no-US post CS-: 4 regressors, 8 events each during acquisition and extinction).

To correct for motion, volume realignment parameters were prepared as six nuisance regressors (three translations and three rotations). Pulse oximetry and respiration data from PMU were processed using essential features of the PhLEM toolbox for SPM (Verstynen and Deshpande, 2011). Heart beat and breathing rate detection were manually verified and if needed corrected. To correct for physiological motion effects the RETROICOR (retrospective image-based correction) method was applied and eight regressors were generated (Glover et al., 2000), resulting in a total of 14 nuisance regressors for each fMRI run.

First level main effect contrasts against rest and differential first level contrasts were generated and tested in second level *t*-tests. The contrast "US post CS+ > no-US post CS-" was calculated to reveal activation in response to the presentation of the aversive stimulus (US). The contrast "CS+ > CS-" was calculated to reveal activation related to the prediction of the US. Finally, the contrast "no-US post CS+ > no-US post CS-" was calculated to reveal activation related to the omission of the US. To evaluate differences between early and late acquisition and extinction, individual second level within-subject ANOVA were modelled for the contrasts "CS+ > CS-" and "no-US post CS+ > no-US post CS-", and (for acquisition only) for the contrast "US post CS+ > no-US post CS-". Threshold-free cluster enhancement (TFCE) was applied using the TFCE toolbox for SPM12 (R164 and R174, http://dbm.neuro.uni-jena.de/tfce/).

In addition, second level one-way ANOVA was modeled for the three main acquisition contrasts (considering early and late acquisition together). To identify regions of shared

activation conjunction analysis (Price and Friston, 1997) was performed to test global null hypotheses for each of the three contrasts. Using the same second level model main effect of contrast was calculated to assess differences between the three contrasts (*F*-test, contrast vector: [1 -1 0; 0 1 -1]).

Psychophysiological interactions were modelled for the whole brain analysis (Friston et al., 1997) using cerebellar volumes of interest (VOI) based on conjunction analysis in SUIT space as seed regions. TFCE was applied on the results. Additionally, region mean β values for selected VOIs were extracted from simple first level β maps against rest and compared between CS and US events using ANOVA and paired *t*-tests.

To display results, cerebellar (SUIT space) activation maps were plotted on cerebellar flatmaps (Diedrichsen and Zotow, 2015). Whole brain MNI space activation maps were projected on MNI152 average T1 volume provided with SPM (icbm_avg_152_t1_tal_lin.nii). Activation maps were masked in SUIT space using the SUIT atlas volume (Cerebellum-SUIT.nii) with the inner-cerebellar white matter manually filled in, and in MNI space using the SPM canonical inner-cranial volume mask (mask_ICV.nii). To acquire anatomical region labels, maps were then projected onto the SUIT atlas volume (Cerebellum-SUIT.nii, Diedrichsen, 2006) and the AAL atlas volume (AAL.nii, Tzourio-Mazoyer et al., 2002), respectively.

Results

Behavioral data

Questionnaires

Valence and arousal ratings: After habituation and prior to acquisition, there was no difference in (hedonic) valence and (emotional) arousal ratings of the CS+ and CS- (**Fig. 2a**). After acquisition, valence of the CS+ was rated less pleasant than of the CS-. Additionally, arousal to the CS+ was rated higher than to the CS-. Differences between CS+ and CS- ratings remained after extinction, a finding that has been reported as resistance to extinction in evaluative conditioning research (e.g. Blechert et al., 2008; Vansteenwegen et al., 2006). ANOVA with repeated measures showed a significant difference within stimulus types and phases (pre-acquisition, post-acquisition, post-extinction) considering both valence and arousal (main effects: all $p < 0.002$). Valence and arousal ratings differed between stimulus type and phases (interaction stimulus type × phase: valence: $F_{2,42} = 14.95$, $p < 0.001$; arousal: $F_{2,42} = 15.30$, $p < 0.001$). Post hoc tests showed a significant difference between stimulus types after acquisition and after extinction (all $p \leq 0.005$; paired t-test), but not prior to acquisition (valence: $p = 0.781$, arousal: $p = 0.125$).

US unpleasantness und CS-US contingency: After acquisition, the mean US unpleasantness rating was 6.9 (SD = 1.4) on a 9-point scale from "not unpleasant" to "very unpleasant". All participants were aware of CS-US contingencies after the acquisition phase: The mean estimated probability that a CS+ was followed by an US was 70.0% (SD = 13.0%). All but one participant estimated a 0% probability of a CS- being followed by a US, with the remaining participant stating a 10% chance. Participants stated that they became aware of CS-US contingencies after 2.9 min (SD = 1.2 min), or 2.6 (SD = 0.8) US events.

Skin conductance responses (SCR)

During habituation, SIR was not significantly different in CS+ and CS- trials ($t_{21} = 0.708$, $p = 0.487$; paired t-test) (**Fig. 2c**). During fear acquisition, SIR was significantly higher in CS+ trials compared to CS- trials (**Fig. 2c**). This difference was most pronounced in the second half of the acquisition phase. ANOVA with repeated measures showed a significant main effect of stimulus type (CS+ vs. CS-; $F_{1,21} = 5.182$, $p = 0.033$) and block (early vs. late;

348 $F_{1,21} = 5.589$, $p = 0.028$). The stimulus type by block interaction was not significant
349 ($F_{1,21} = 1.409$, $p = 0.249$).

350 During fear extinction, SIR related to the CS+ declined. In the second half of extinction the
351 difference between CS+ and CS- trials vanished (**Fig. 2c**). The main effects of stimulus type
352 (CS+ vs. CS-; $F_{1,21} = 2.923$, $p = 0.102$) and block (early vs. late; $F_{1,21} = 3.930$, $p = 0.061$) were
353 not significant. ANOVA with repeated measures showed a significant stimulus type by block
354 interaction ($F_{1,21} = 5.035$, $p = 0.036$). Post hoc testing showed a significant difference
355 between stimulus type during early ($t_{21} = 2.24$, $p = 0.036$), but not during late extinction
356 ($t_{21} = -0.36$, $p = 0.723$).

357 Findings concerning FIR were comparable to SIR and are summarized in **Supplement (Supp.)**
358 **Fig. 1** and **Table 1**.

359 SCRs in the unconditioned response (UR) window (i.e. the third interval response, TIR) were
360 significantly higher in paired CS+ trials (US post CS+) compared to CS- trials (no-US post CS-)
361 ($F_{1,21} = 93.70$, $p < 0.001$) indicating a successful increase in SCR towards the electric shock
362 (**Fig. 2d**). Block effect was significant (early vs. late; $F_{1,21} = 21.97$, $p < 0.001$) revealing higher
363 UR during early compared to late acquisition. The block by stimulus type interaction was not
364 significant ($F_{1,21} = 0.75$, $p = 0.396$). TIR was also significantly higher in unpaired CS+ trials
365 (no-US post CS+) compared to CS- trials (no-US post CS-) during late acquisition ($t_{21} = 3.72$,
366 $p = 0.001$) but not early acquisition ($t_{21} = 1.74$, $p = 0.096$), showing a higher US expectancy in
367 US omission trials. TIR in unpaired CS+ trials was significantly smaller compared to TIR in
368 paired CS+ trials (paired *t*-tests, all *p* values < 0.001). During extinction, TIR was not
369 significantly different comparing stimulus types (no-US post CS+ vs. no-US post CS-;
370 $F_{1,21} = 3.46$, $p = 0.077$), blocks (early vs. late; $F_{1,21} = 3.72$, $p = 0.067$) or their interaction
371 (stimulus type by block; $F_{1,21} = 0.02$, $p = 0.878$).

372 Taken together, we could show successful fear acquisition and extinction as well as a
373 response towards the presentation and the omission of the US during fear acquisition.

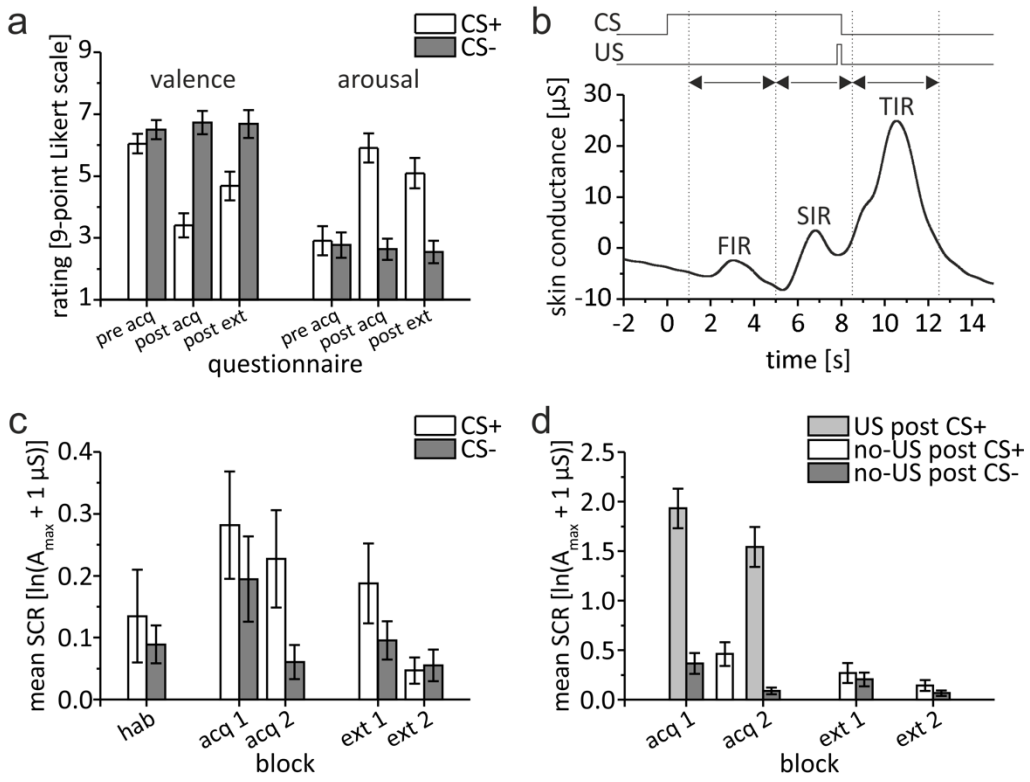

Figure 2: Behavioral data. **a)** Group mean valence and arousal ratings for CS+ and CS- during acquisition and extinction. **b)** Example of bandpass filtered individual skin conductance response (SCR) in a paired CS+/US trial depicting response interval windows and displaying a distinct response in each interval. **c)** Group mean second interval response (SIR). **d)** Group mean third interval response (TIR). Please note the different scales of the y-axis used for illustration purposes. Error bars represent standard errors of the mean. hab = habituation, acq 1, acq 2 = early and late acquisition, ext 1, ext 2 = early and late extinction.

fMRI data

We were interested in cerebellar activations related to i) the presentation, ii) the prediction, and iii) the omission of the aversive electrical stimulation (that is, the US). Focus of data analysis was on cerebellar activations. In addition, exploratory data on whole brain analysis is presented. Activation clusters are reported which are significant after application of threshold-free cluster-enhancement (TFCE) at $p < 0.05$ familywise error (FWE) corrected level.

Cerebellar analysis

Cerebellar activation related to the presentation of the aversive stimulus [contrast "US post CS+ > no-US post CS-"]: Widespread cerebellar activation was observed within the cerebellar vermis and both cerebellar hemispheres (**Fig. 3a**; see also **Table 1**). Most prominent differential activations were found in the anterior and posterior vermis (local maxima in lobules I-IV, V) and the left hemisphere (that is ipsilateral to the presentation of the US; local maximum in Crus I). Activation was not confined to the cerebellar cortex, but extended into the cerebellar nuclei (including dentate, interposed and fastigial nuclei bilaterally).

To assess changes in differential cerebellar activation across the two acquisition blocks (early and late) an *F*-test based on second level within-subject ANOVA was calculated. No significant main effect of block was observed during acquisition (at $p < 0.05$ FWE corrected level, based on the TFCE statistic).

Cerebellar activation related to the prediction of the aversive stimulus [contrast "CS+ > CS-"]: Cerebellar activation related to the CS+ was significantly higher in the lateral cerebellar hemispheres compared to activation related to the CS- (**Fig. 3b**). Cerebellar activation was present in the more lateral parts of lobules VI and Crus I bilaterally (see also **Table 1**). Additional differential activation was present in lobules VIIIa and VIIIb in the right cerebellar hemisphere. During extinction, cerebellar activation related to the CS+ was not significantly different from activation related to the CS- (at $p < 0.05$ FWE corrected level, based on the TFCE statistic).

F-tests revealed no significant block effects (early vs. late) neither during acquisition nor during extinction (at $p < 0.05$ FWE corrected level, based on the TFCE statistic). The main

412 effect of block across all four blocks (that is early and late acquisition, early and late
413 extinction) revealed two clusters in the lateral cerebellum with local maxima in left lobule
414 Crus I and right lobule VI (**Table 1; Supp. Fig. 2a**). As can be seen from mean *β* values of both
415 clusters across blocks (see insert in **Supp. Fig. 2a**), differential activation in the two clusters
416 decreased during extinction compared to acquisition.

417 *Cerebellar activation related to the omission of the aversive stimulus [contrast "no-*
418 *US post CS+ > no-US post CS-"]*: During acquisition, significant differential activation related
419 to the (unexpected) omission of the US was found in the cerebellar hemispheres and the
420 vermis (**Fig. 3c**). Activation at the time of the expected US in unpaired CS+ trials compared to
421 CS- trials was most prominent in the left cerebellar hemisphere with local maxima in lobules
422 Crus I and VI (**Table 1**). Additional activation was present in the right hemisphere (local
423 maxima in lobules Crus I and VI) and the vermis. Vermal activation was found in the anterior
424 vermis (lobules I-IV, V) and the posterior vermis (lobules VIIb-IX). Activation extended into
425 the cerebellar nuclei (including dentate, interposed and fastigial nuclei bilaterally). During
426 extinction, cerebellar activation related to the (expected) omission of the US strongly
427 decreased. Only one smaller cluster remained in more medial parts of left Crus I (**Table 1**;
428 **Supp. Fig. 2c**).

429 *F*-tests revealed no significant block effects (early vs. late) neither during acquisition nor
430 during extinction (at $p < 0.05$ FWE corrected level, based on the TFCE statistic). The main
431 effect of block across all four blocks (that is early and late acquisition, early and late
432 extinction) revealed a large cluster in the left hemisphere, primarily within lobule Crus I with
433 some extension to lobule VI and Crus II (**Table 1; Supp. Fig. 2b**). As can be seen from mean *β*
434 values across blocks (insert in **Supp. Fig. 2b**), differential activation decreased during
435 extinction compared to acquisition.

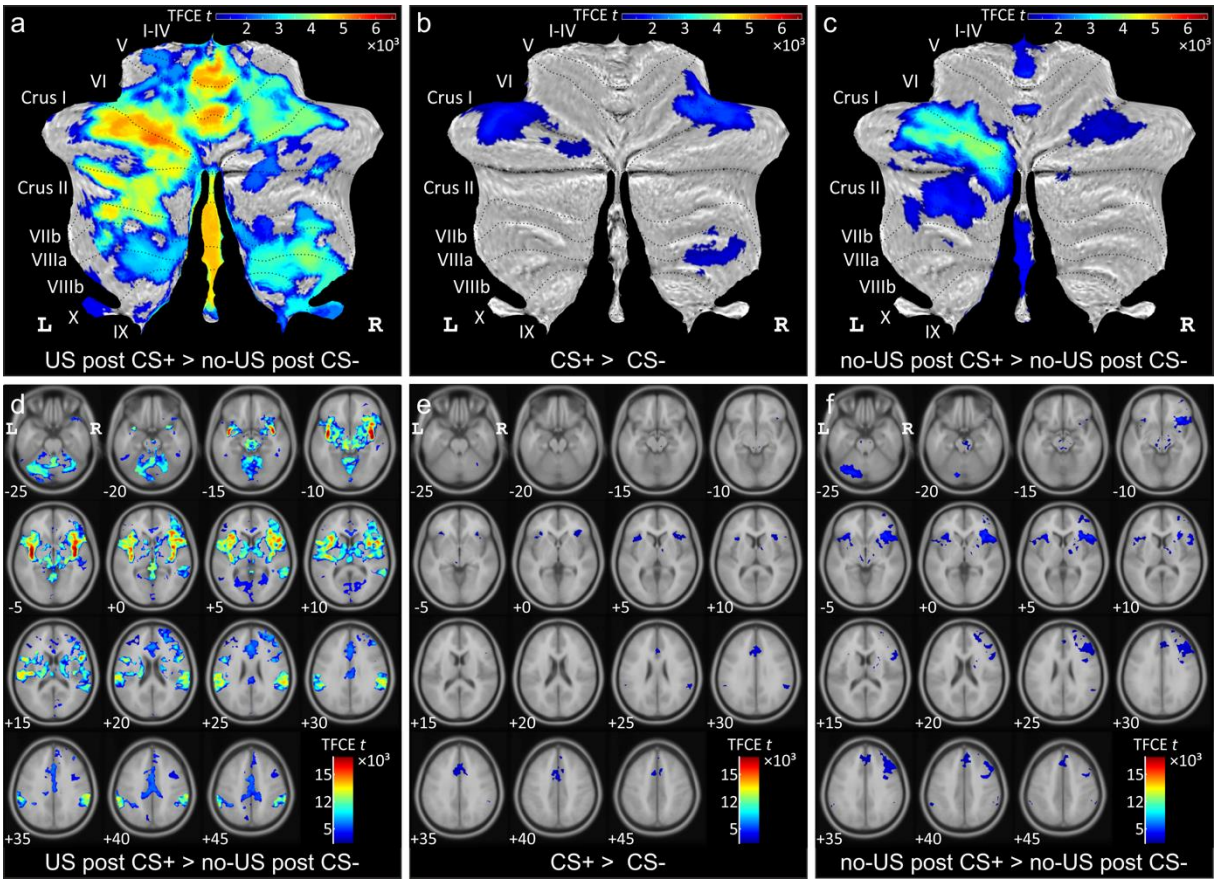

Figure 3: (a-c) Differential cerebellar activations during fear acquisition in SUIT space projected on a cerebellar flatmap (Diedrichsen and Zotow, 2015). **(d-f)** Corresponding differential whole brain activations in MNI normalized space. All contrasts calculated using TFCE and familywise error correction ($p < 0.05$). L = left, R = right

Table 1: Cerebellar activations during acquisition and extinction. Displayed are all clusters of 20 mm^3 and larger. In each cluster, up to three maxima are listed separated by 8 mm or more. Corresponding activations for whole brain analysis are summarized in **Supp. Table 5**.

Index	Location (lobule)	Side	SUIT coordinates / mm			Cluster size / mm^3	p_{FWE}	TFCE
a) US post CS+ > no-US post CS- : acquisition	***t-test, TFCE, p < 0.05, FWE corr.***							
1	Extended cluster	left VI (8390), white matter (7950), left Crus I (7889), right VI (6404), right V (4250), left Crus II (4223), left V (4085), right Crus I (3457), right I-IV (2761), left I-IV (2529), right VIIIa (2432), right VIIIb (2244), left VIIb (1602), left VIIIb (1583), left VIIIa (1536), right VIIb (1467), vermal VI (1368), right IX (1330), vermal VIIIa (1307), right Crus II (1034), right dentate nuc. (921), vermal IX (804), left dentate nuc. (713), left IX (628), vermal VIIIb (474), vermal VIIb (236), right X (168), vermal Crus II (162), vermal X (120), left interposed nuc. (86), left X (70), right interposed nuc. (69), left fastigial nuc. (23), vermal Crus I (21), right fastigial nuc. (19)						
	Crus I	Left	-26	-74	-27	72355	0.001	5386.8
	I-IV	Left	0	-53	-24		0.001	5373.2
	V	Left	-3	-62	-23		0.001	5032.2
2	IX	Left	-5	-47	-51	39	0.025	1592.2
3	IX	Right	7	-49	-61	117	0.034	1435.8
b) CS+ > CS- : acquisition	***t-test, TFCE, p < 0.05, FWE corr.***							
1	Extended cluster	right Crus I (1506), right VI (1481), white matter (23), right V (16)						
	VI	Right	35	-50	-31	3027	0.004	2256.6
	VI	Right	33	-60	-26		0.004	2174.7
	Crus I	Right	40	-57	-32		0.005	2082.8
2	Extended cluster	left Crus I (1658), left VI (727)						
	Crus I	Left	-44	-56	-33	2385	0.006	1911.7
	Crus I	Left	-36	-53	-33		0.007	1851.3
	Crus I	Left	-41	-64	-31		0.014	1629.8
3	Extended cluster	right VIIIa (287), right VIIIb (283), white matter (36), right VIIb (2)						
	VIIIb	Right	28	-48	-49	608	0.019	1495.2
	VIIIb	Right	22	-54	-48		0.020	1483.1
	VIIIa	Right	29	-58	-47		0.037	1263.4
4	Crus I	Left	-17	-76	-29	264	0.036	1278.4
5	Crus I	Left	-34	-75	-25	46	0.047	1163.4
c) CS+ > CS- : extinction	***t-test, TFCE, p < 0.05 FWE corr.***							
	no significant voxels							
d) no-US post CS+ > no-US post CS- : acquisition	***t-test, TFCE, p < 0.05, FWE corr.***							
1	Extended cluster	left Crus I (7688), left VI (4023), left Crus II (3373), white matter (1741), right I-IV (580), left VIIb (541), left dentate nuc. (474), left I-IV (472), vermal VIIIb (226), vermal IX (200), right interposed nuc. (163), vermal VIIIa (159), right dentate nuc. (92), left interposed nuc. (73), right V (70), left V (41), left IX (34), right fastigial nuc. (31), left VIIIa (30), vermal VI (9), right IX (9), vermal Crus I (8), left fastigial nuc. (8), vermal Crus II (2)						
	Crus I	Left	-17	-78	-25	20047	< 0.001	4010.8
	VI	Left	-25	-73	-26		< 0.001	3912.9
	Crus I	Left	-41	-68	-29		0.001	3633.1
2	Extended cluster	right Crus I (1313), right VI (750), white matter (66)						

		VI	Right	30	-68	-27	2129	0.015	1484.6
		VI	Right	25	-73	-22		0.018	1422.4
		Crus I	Right	45	-65	-27		0.019	1384.5
	3	Crus II	Right	15	-79	-33	42	0.047	1079.1
e)	***no-US post CS+ > no-US post CS- : extinction***			***t-test, TFCE, p < 0.05, FWE corr.***					
	1	Crus I	Left	-14	-72	-35	273	0.016	1416.9

445

446

Comparison of cerebellar areas related to the presentation, the prediction and the omission of the aversive stimulus

Conjunction analyses were performed to reveal areas of cerebellar activation which were common to the presentation, the prediction and the (unexpected) omission of the aversive US during acquisition (based on the three differential contrasts reported above). Conjunction analyses revealed common areas of activation in the cerebellar hemispheres primarily on the left (local maxima Crus I; testing global null hypotheses at a threshold of $p < 0.05$ FWE corrected level without TFC enhancement) (**Fig. 4a,** see also **Supp. Table 2**). Additional common areas of cerebellar activation were present in the anterior and posterior vermis when considering the two contrasts related to US presentation and its unexpected omission only (**Supp. Fig. 3b**).

Next, we were interested whether the level of activations differed between the three differential contrasts of interest. Using the same second level model, the main effect of contrasts was calculated (*F*-test, contrast vector: [1 -1 0; 0 1 -1]; $p < 0.05$ FWE corrected without TFC enhancement). Significant differences were found in the left lobule Crus I (with a small extension into lobule VI) and a small cluster in the anterior vermis (local maximum lobule I-IV) (**Fig. 4b**, **Supp. Table 3**). This difference reflected a lower level of activation related to the prediction of the aversive stimulus compared to its presentation and unexpected omission (see small insert in **Fig. 4b**). Comparing any two out of the three contrasts at a time, revealed no significant difference in the level of activations comparing the omission and the prediction of the aversive stimulus, except a small cluster in the anterior vermis which was more prominent related to the omission of the US (**Supp. Fig. 3e**). The level of activations of the vermis and neighboring areas of the cerebellar hemispheres were significantly higher related to the experience of the US compared to its prediction and unexpected omission (**Supp. Fig. 3d,e).**

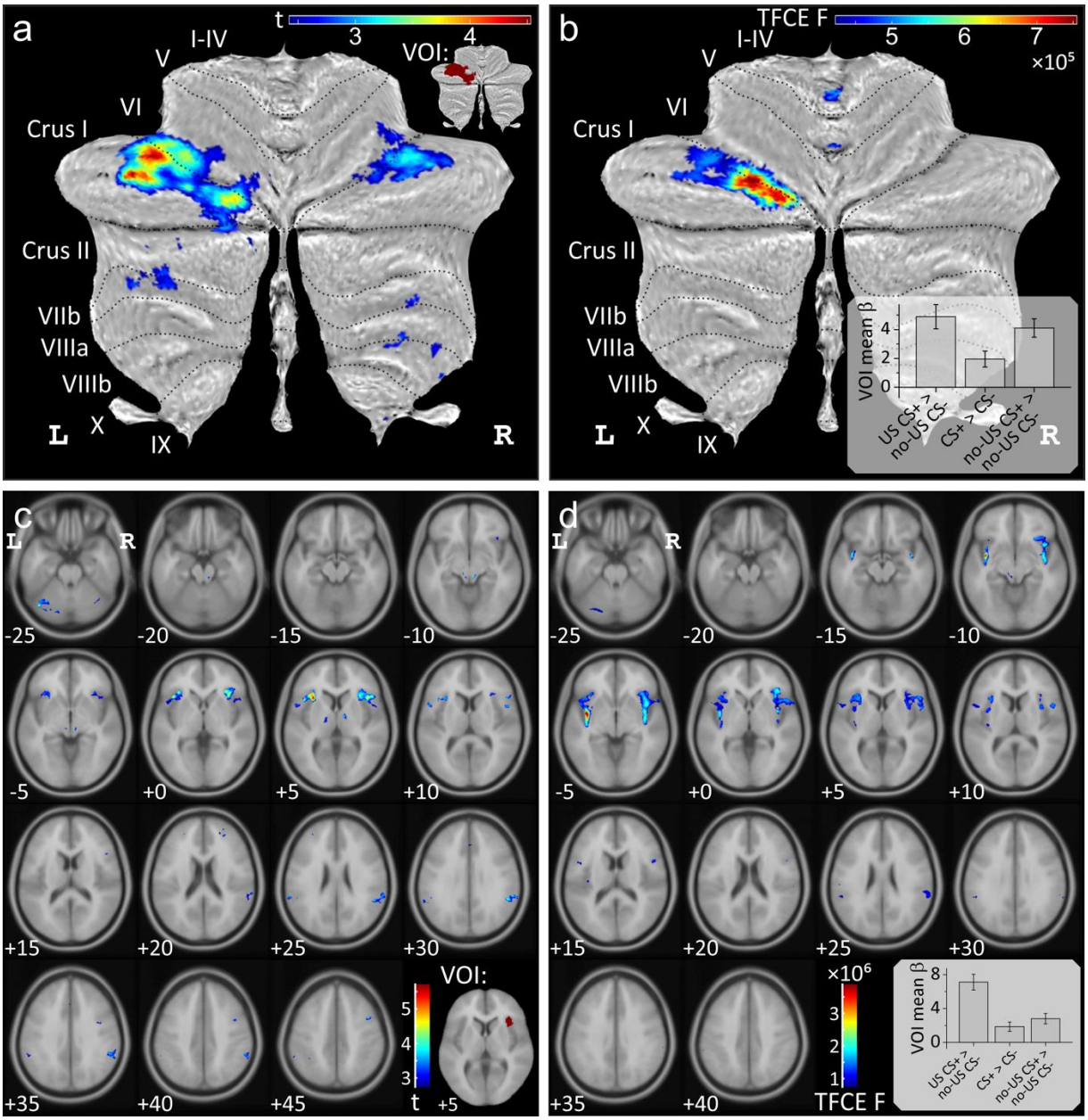

Figure 4: Conjunction analyses testing global null hypotheses (**a,c**) and analyses of differences (**b,d**) between the three contrasts "US post CS+ > no-US post CS-", "CS+ > CS-" and "no-US post CS+ > no-US post CS-" (shown in **Fig. 3**) during fear acquisition. Data in (**a,b**) is shown in SUIT space and in (**c,d**) in MNI space. All contrasts displayed using FWE correction ($p < 0.05$), (**b,d**) using TFCE. Bar graphs display group mean β values for each contrast considering the whole activation volume (error bars: standard error). Volumes of interests (VOI) were defined based on conjunction analyses and are shown in the inserts: cerebellar VOI (**a**) and insula VOI (**c**).

Mean β values related to each event (presentation of US, CS+, CS-, omission of US) compared to rest

Based on the conjunction analyses for the three contrasts of interest in acquisition, we defined a volume of interest (VOI) in the left cerebellar hemisphere (indicated in red in the insert in **Fig. 4a**). Mean *β* values were calculated for each event compared to rest within the VOI.

During acquisition, mean *β* values in CS+ trials (black triangles in **Fig. 4a**) were significantly higher compared to CS- trials (inverted gray triangles; $F_{1,21} = 14.56$, $p = 0.001$). The block (early vs. late) effect ($F_{1,21} = 0.64$, $p = 0.432$) and stimulus type by block interaction ($F_{1,21} = 3.96$, $p = 0.060$) effects were not significant. During extinction, mean *β* values declined in CS+ trials, and were no longer different between CS+ and CS- trials ($F_{1,21} = 0.27$, $p = 0.610$). Block ($F_{1,21} = 3.94$, $p = 0.060$) and stimulus type by block interaction ($F_{1,21} < 0.01$, $p = 0.973$) effects were not significant.

Mean *β* values related to US events were significantly higher in response to the presentation of the aversive US in paired CS+ trials (US post CS+; black diamonds in **Fig. 5a**) compared to the corresponding event in CS- trials (no-US post CS-; inverted black triangles) ($F_{1,21} = 26.75$, $p < 0.001$). There were no significant block (early vs. late; $F_{1,21} = 2.22$, $p = 0.151$) or stimulus type by block interaction effects ($F_{1,21} < 0.01$, $p = 0.960$). Likewise, mean *β* values related to the unexpected omission of the US in CS+ trials (no-US post CS+; gray triangles) were significantly higher compared to the corresponding event in CS- trials in early ($t_{21} = 4.38$, $p < 0.001$) and late acquisition phase ($t_{21} = 6.73$, $p < 0.001$). During extinction, mean *β* values declined, but remained significantly higher related to no-US post CS+ events compared to no-US post CS- events ($F_{1,21} = 4.52$, $p = 0.046$). The block effect (early vs. late; $F_{1,21} = 8.326$, $p = 0.009$) was significant. The stimulus type by block interaction was not significant ($F_{1,21} = 0.08$, $p = 0.784$).

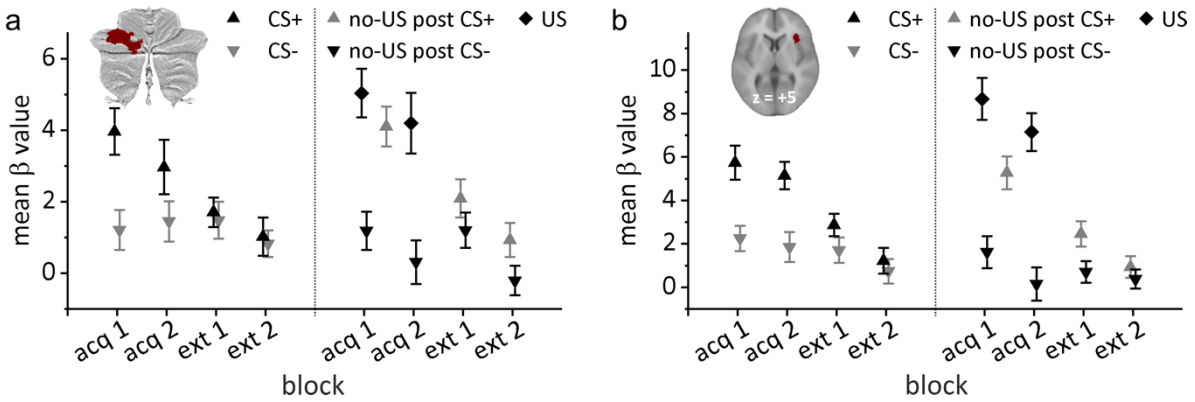

Figure 5: Group mean β values related to each event (presentation of US, CS+, CS-, omission of US) compared to rest. **a)** Volume of interest (VOI) in the left cerebellar hemisphere; **b)** VOI in the right insula. Error bars represent standard errors. hab = habituation, acq 1, acq 2 = early and late acquisition, ext 1, ext 2 = early and late extinction.

PPI data: cerebello-cerebral interactions

As described above, a VOI was defined in the lateral cerebellar cortex based on conjunction analyses. Analyses of psychophysiological interactions (PPI) for the three contrasts of interest were performed between this cerebellar VOI and the whole brain. PPIs are reported which are significant at $p < 0.05$ FWE corrected level after TFCE application. The most prominent finding was significant modulation of the functional connectivity between the cerebellum and occipital lobe during fear acquisition. There was no significant PPI found during extinction.

PPI related to the presentation of the aversive stimulus. Considering the seed region in the left cerebellar hemisphere, activation related to the presentation of the US (as revealed by the contrast "US post CS+ > no-US post CS-") showed increased functional connectivity with striate and extrastriate visual areas (blue-green color code in **Fig. 6**; see also **Table 2;** local maxima in the calcarine fissure and surrounding cortex (V1)). Additional areas of increased functional connectivity were found in limbic areas (cingulum, parahippocampus). No significant decreases of functional connectivity were found.

PPI related to the prediction of the aversive stimulus. Cerebellar activation in the hemispherical seed region related to the prediction of the aversive stimulus (as revealed by the contrast "CS+ > CS-") showed increased functional connectivity with extrastriate visual

areas (local maxima in middle occipital lobe, lingual gyrus, fusiform gyrus; red-yellow color code in **Fig. 6**; **Table 2**). No significant decreases of functional connectivity were found.

PPI related to the (unexpected) omission of the aversive stimulus. Cerebellar activation in the in the hemispherical seed region related to the (unexpected) omission of the aversive US (as revealed by the contrast "no-US post CS+ > no-US post CS-") showed no significant increases or decreases of functional connectivity.

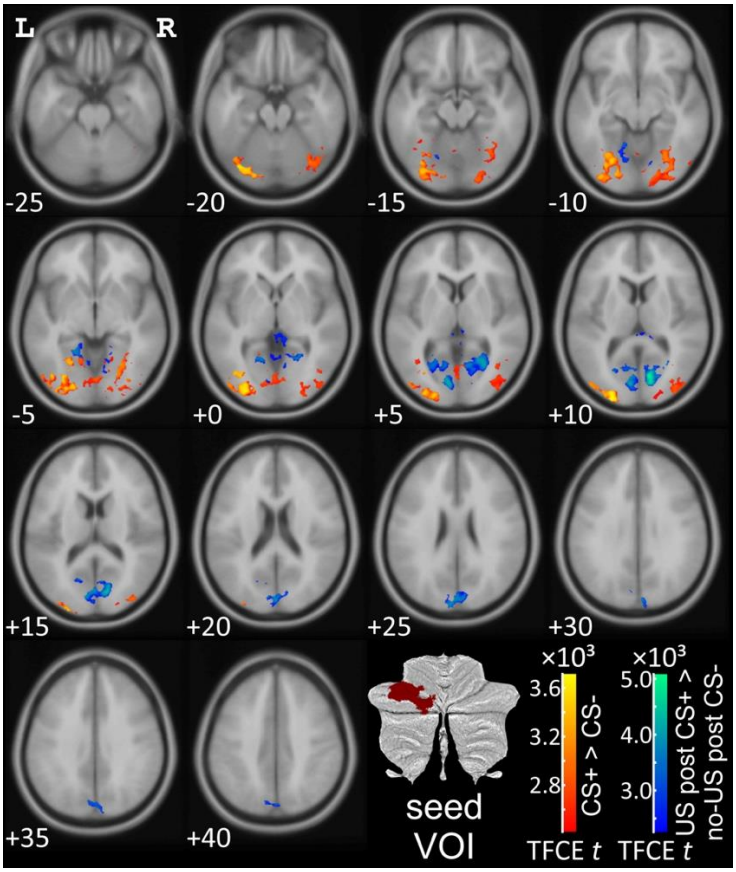

Figure 6: Psychophysiological interaction (PPI) analysis based on a seed region in the left lateral cerebellar cerebellum ($p < 0.05$ FWE corrected level after TFCE application). L = left, R = right.

Table 2: Psychophysiological interactions (PPI) based on a seed region in the left lateral cerebellum. Clusters of 20 mm^3 or larger are shown. Up to three maxima in each cluster are shown separated by at least 8 mm.

Index	Location	Side	SUIT coordinates / mm			Cluster size / mm^3	p_{FWE}	TFCE
PPI (increased functional connectivity): acquisition, US post CS+ > no-US post CS-			***t-test, TFCE, p < 0.05 FWE corr.***					
1	Extended cluster	right Calcarine (4607), left Calcarine (3955), left Cuneus (2921), left Lingual (1995), right Lingual (1903), outside GM (1632), right Cuneus (932), left Precuneus (424), vermal Lob. IV-V (323), left Lob. IV-V (193), left Lob. VI (141), left Occipital_Sup (117), right Thalamus (53), right Precuneus (47), left Thalamus (39), right Lob. IV-V (37), right Cingulum_Post (27), left Parietal_Sup (27), left Cingulum_Post (13), left ParaHippocampal (11), right Hippocampus (9), right ParaHippocampal (3)						
	Calcarine	Right	11	-74	11	19409	0.001	5080.1
	Calcarine	Left	-8	-80	7		0.002	4220.7
	Calcarine	Right	22	-58	3		0.003	4102.5
PPI (increased functional connectivity): acquisition, CS+ > CS-			***t-test, TFCE, p < 0.05 FWE corr.***					
1	Extended cluster	left Occipital_Mid (5908), left Lingual (4253), left Fusiform (2706), left Occipital_Inf (2297), outside GM (1491), left Lob. Crus I (645), right Lingual (616), left Calcarine (241), left Lob. VI (177), left Occipital_Sup (114), right Calcarine (99), left Precuneus (21), left Temporal_Mid (16), vermal Lob. IV-V (3)						
	Occipital_Mid	Left	-24	-98	10	18587	0.007	3714.2
	Occipital_Mid	Left	-29	-89	0		0.008	3634.5
	Fusiform	Left	-24	-71	-8		0.009	3568.4
2	Extended cluster	right Fusiform (3493), right Occipital_Mid (2820), right Lingual (2743), right Occipital_Inf (1068), outside GM (1040), right Temporal_Mid (411), right Occipital_Sup (329), right Cuneus (301), right Lob. Crus I (288), right Lob. VI (270), right Temporal_Inf (251), right Calcarine (151)						
	Fusiform	Right	33	-79	-7	13165	0.018	3160.4
	Lingual	Right	26	-62	-6		0.018	3133.8
	Fusiform	Right	24	-71	-6		0.02	3088.5
3	Paracentralobule	Left	-2	-38	69	394	0.018	3158.1
4	Extended cluster	vermal Lob. IV-V (92), left Lob. IV-V (35), vermal Lob. VI (12), left Lob. VI (8)						
	Lob. VI	Vermal	-1	-64	-10	147	0.04	2580.3
	Lob. IV-V	Vermal	1	-56	-4		0.05	2417.9
5	Extended cluster	left Fusiform (248), left Occipital_Inf (6), outside GM (1), left Temporal_Inf (1)						
	Fusiform	Left	-33	-48	-13	256	0.042	2541.9
	Fusiform	Left	-41	-58	-14		0.042	2520.3
6	Extended cluster	right Lingual (173), right Lob. IV-V (14)						
	Lingual	Right	17	-56	-4	187	0.044	2483.6
	Lingual	Right	10	-60	-4		0.045	2475.6
7	Lingual	Right	17	-52	2	65	0.047	2455.3

Whole brain analysis

Although the focus of the study was on the cerebellum, exploratory whole brain fMRI analysis was also performed. Data is presented at $p < 0.05$ FWE corrected level after TFCE application. Most prominent activation was observed within the insula (**Fig. 3**). Activation of other limbic areas was observed primarily related to the presentation of the aversive stimulus. Similar to cerebellar activation, prominent activation of the insula was observed not only to the prediction of the upcoming US but also related to its unexpected omission during acquisition trials. Cerebral activations vanished during extinction trials (at $p < 0.05$ FWE corrected level after TFCE).

Cerebral activation related to the presentation of the aversive stimulus [contrast "US post CS+ > no-US post CS-"]: Most prominent activations were found in the insula bilaterally (**Fig. 3d**). Additional differential activations were present in the anterior and middle cingulate gyrus, the amygdala, supplementary motor area (SMA), supramarginal and superior temporal gyrus bilaterally, frontal inferior gyrus and cuneus (summarized in **Supp. Table 5**).

Cerebral related to the prediction of the aversive stimulus [contrast "CS+ > CS-"]: During acquisition, cerebral activation related to the CS+ was significantly higher compared to the CS- in the more anterior parts of the insula bilaterally (**Fig. 3e; Supp. Table 5**). Additional differential activation was present in the right SMA and middle cingulate gyrus. During extinction, no significant fMRI activation was observed.

Cerebral activation related to the omission of the aversive stimulus [contrast "no-US post CS+ > no-US post CS-"]: During acquisition, significant differential activation related to the (unexpected) omission of the US was found in more anterior parts of the insula bilaterally (**Fig. 3e, Supp. Table 5**). Additional activation was found bilaterally in the SMA, anterior and medial cingulate and right supramarginal cortex. During extinction, no significant activations were observed.

Comparison of cerebellar areas related to the presentation, the prediction and the omission of the aversive stimulus

Conjunction analyses revealed that the more anterior parts of the insula bilaterally were activated in the three contrasts of interest (testing the global null hypotheses at a threshold

of $p < 0.05$ FWE corrected level without TFC enhancement) (**Fig. 4c,** see also **Supp. Table 2**). In the anterior, but also posterior parts of the insula the level of activations differed between the three differential contrasts of interest (*F*-tests; $p < 0.05$ FWE corrected without TFC enhancement; **Fig. 4d**, **Supp. Table 3**). This difference reflected a higher level of activation related to the experience of the aversive stimulus compared to its prediction and unexpected omission (see small insert in **Fig. 4d**).

Mean β-values in the insula related to each event (presentation of US, CS+, CS-, omission of US) compared to rest

A VOI was defined in the insula based on conjunction analyses considering the three contrasts of interest as described above (see insert in **Fig. 4c**). We choose the right insula because the left cerebellar hemisphere is connected with the right cerebral hemisphere.

During acquisition, mean *β* values in CS+ trials (black triangles in **Fig. 5b**) were significantly higher than in CS- trials (inverted gray triangles; $F_{1,21} = 17.97$, $p < 0.001$). The block effect (early vs. late; $F_{1,21} = 1.14$, $p = 0.298$) and stimulus type by block interaction ($F_{1,21} = 0.05$, $p = 0.825$) effects were not significant. During extinction, mean *β* values in CS+ trials declined. The block effect was significant ($F_{1,21} = 6.69$, $p = 0.017$). Stimulus type ($F_{1,21} = 1.64$, $p = 0.215$) and stimulus type by block interaction effects ($F_{1,21} = 0.51$, $p = 0.483$) were not significant.

Mean *β* values in the VOI in the right insula were significantly higher in response to the presentation of the aversive US in paired CS+ trials (US post CS+; black diamonds in **Fig. 5b**) compared to the corresponding event in CS- trials (no-US post CS-; inverted black triangles) ($F_{1,21} = 38.09$, $p < 0.001$). The block effect was significant (early vs. late; $F_{1,21} = 9.05$, $p = 0.007$). The stimulus type by block interaction was not significant ($F_{1,21} < 0.01$, $p = 0.947$). Likewise, mean *β* values related to the unexpected omission of the US in CS+ trials (no-US post CS+; gray triangles) were significantly higher compared to the CS- trials in early ($t_{21} = 4.30$, $p < 0.001$) and late acquisition ($t_{21} = 5.09$, $p < 0.001$). During extinction, mean *β* values at the time of the presentation of the US in CS+ trials declined, but remained higher compared to CS- trials in early extinction. Stimulus type effect was significant ($F_{1,21} = 5.60$, $p = 0.028$). Block ($F_{1,21} = 3.95$, $p = 0.060$) and stimulus type by block interaction ($F_{1,21} = 0.08$, $p = 0.784$) effects were not significant.

Discussion

Cerebellar activation was observed related to the learned association of the CS and the aversive US confirming previous results (Fischer et al., 2000; Frings et al., 2002; Ploghaus et al., 1999). Most importantly, marked cerebellar activation was found also during the unexpected omission of the unpleasant event and disappeared during extinction trials (in which the omission became expected). These findings support the hypothesis that the cerebellum acts as or is part of a predictive device not only in the motor but also in the emotional domain. In addition to the cerebellum, exploratory whole brain analysis showed very similar patterns of activation in the insula, which has been shown to be involved in aversive prediction error processing by others (Geuter et al., 2017; Li et al., 2011). Thus, first evidence was found that the cerebellum is part of a more extended neural network processing prediction errors in learned emotional responses. The discussion will focus on the cerebellar findings, which were also accompanied by changes in functional connectivity predominantly with visual cortices. Hence, one cerebellar role in emotional control may be to modulate processing of fear-related sensory information.

Cerebellar activation during the presentation and the prediction of aversive events

Cerebellar activation during the presentation and the prediction of aversive events is in good accordance with the literature (Dimitrova et al., 2003; Lange et al., 2015; Maschke et al., 2003; Ploghaus et al., 1999). In a seminal study, Ploghaus et al. (1999) reported that distinct, but closely adjacent cerebellar areas were related to the experience and the prediction of pain. In accordance, we found activation of the anterior cerebellum with a maximum in the cerebellar vermis related to presentation of the aversive stimulus. Different to Ploghaus et al. (1999), however, cerebellar activation related to the experience of the US showed a significant extension to the posterolateral cerebellum (including lobules Crus I and VI) and overlapped with the area related to the prediction of the aversive stimulus. Furthermore, the level of activation in the posterolateral cerebellum was more related to the experience of the aversive stimulus compared to its prediction. Likewise, other fMRI studies have reported that aversive stimuli result in more widespread cerebellar activations of both anteromedial and posterolateral areas (painful electrical stimulation of the feet: Dimitrova et al., 2003; airpuffs directed to the eye: Maschke et al., 2003; Moulton et al., 2010). Responses

635 to aversive stimuli are complex and involve autonomic, sensorimotor, and higher-order
636 emotional reactions. Parts of the vermis are known to contribute to autonomic functions
637 (Apps and Strata, 2015 for reviews; Apps et al., 2018), the anterior lobe, part of lobule VI and
638 lobule VIII to sensorimotor functions, and lobules Crus I and II to cognitive functions (King et
639 al., 2018; Stoodley and Schmahmann, 2018). Thus, different parts of the cerebellum likely
640 contribute to the various aspects involved in processing of aversive stimuli (Moulton et al.,
641 2010).

642 Very similar to our findings, a more recent fMRI study also reported an overlap of cerebellar
643 areas related to the experience and prediction of painful stimuli in Crus I and lobule VI of the
644 posterolateral cerebellum (Welman et al., 2018). Nevertheless, we suggest a different
645 interpretation of the data than Ploghaus and colleagues (1999): Rather than reflecting a
646 dissociation between the experience and the prediction of unpleasant events, midline parts
647 of the cerebellum are likely involved in autonomic processes, and posterolateral parts of the
648 cerebellum in higher-order emotional processes related to the experience and prediction of
649 potentially harmful stimuli. The known motor areas also likely contribute to this picture.
650 Depending on stimulus intensity participants may withdraw their hand or at least prepare a
651 hand movement. In fact, early animal, but also human cerebellar lesion studies highlight the
652 involvement of the cerebellar vermis in the conditioning of autonomic fear responses (Apps
653 and Strata, 2015 for reviews; Apps et al., 2018; Sacchetti et al., 2002; Supple and Leaton,
654 1990; Supple and Kapp, 1993). For example, Maschke et al. (2002) found than fear-
655 conditioned bradycardia was impaired in patients with lesions of the cerebellar midline but
656 not the lateral cerebellar hemispheres. On the other hand, activation of the posterolateral
657 cerebellar hemisphere is very common in human fear conditioning fMRI studies (Lange et al.,
658 2015). Given the known reciprocal connections of the posterolateral cerebellum and its
659 output nuclei, the dentate nuclei, with the prefrontal cortex (Middleton and Strick, 1994;
660 Middleton and Strick, 2000), lateral activations may reflect the more cognitive aspects of
661 emotional processing. In the present study, the focus of activation was within Crus I with
662 some extension into lobule VI. Although it cannot be excluded that part of the activation is
663 related to the preparation or subliminal execution of a withdrawal movement, motor-
664 related processes are unlikely to explain the bulk of posterolateral activation. Hand and
665 finger movements result in fMRI activation of ipsilateral lobule V, with additional activation

of lobule VI bilaterally in more complex movements (King et al., 2018; Schlerf et al., 2010). Although some extension to Crus I has been observed in the latter, movements never result in activations primarily of Crus I. Rather, focus of activation is always on lobules V and VI, which was clearly not the case in the present study. Of note, preparation and execution of movements have been found to activate the same cerebellar areas (Cui et al., 2000).

The present findings agree with the classic view that prediction depends on activity in the same networks that process the actual experience (e.g. James, 1892), at least at the level of the cerebellum. Recent single-cell recording studies within the cerebellar cortex in monkeys are also in line with this assumption: Both simple and complex spike firing rates at the same Purkinje cell encode movement kinematics and sensory feedback, but also motor predictions (Popa et al., 2012; Streng et al., 2017a; Streng et al., 2017b).

Based on animal and human lesion data, vermal activation is to be expected related to the prediction of the aversive stimulus. A recent fMRI meta-analysis indeed showed activations of both the cerebellar hemispheres and the vermis in fear conditioning paradigms in healthy humans (Lange et al., 2015). This was, however, neither the case in the present study nor in the study by Ploghaus and colleagues (1999). Because participants were instructed about the CS-US contingencies to a certain degree in both studies, the cognitive component may have had the strongest impact on the fMRI data.

Ploghaus and colleagues (1999) reported a similar dissociation for the experience and the prediction of pain in posterior and anterior parts of the insula, respectively. In the present study, we also found activation related to the US in the posterior insula, and activation related to the CS+ (and therefore prediction of the US) in more anterior parts. Very similar to our cerebellar findings, however, US-related activation extended into the more anterior insula and overlapped with CS+ related activations. Again, we hypothesize that this is not a dissociation between experience and prediction but reflects different functional aspects of processing of potentially harmful stimuli. For example, Frot et al. (2014) suggested that posterior parts of the insula may be more important in the evaluation of the intensity and localization of an aversive stimulus, whereas the anterior insula may process the emotional reaction to the stimulus. However, as yet, the anterior insula, but not the posterior insula has been shown to be involved in processing predictions of aversive events (Geuter et al.,

2017). Notwithstanding, this concept may also be extended to other brain areas, e.g. the medial and anterior cingulate cortex (Vogt, 2014). In the present study, however, no other cerebral regions showed significant activations related to the prediction of the aversive stimulus in the whole brain analysis using a conservative statistical threshold.

Cerebellar activation during the unexpected omission of predicted aversive events

We found cerebellar activation related to the predicted occurrence of an aversive US. More prominent cerebellar activations, however, were observed during the unexpected omission of the unpleasant event. Cerebellar activation was most marked in the posterolateral cerebellum (lobules Crus I, VI), but additional activations were also present in the vermis. Importantly, cerebellar activation vanished during extinction trials, during which the omission of the US became expected. These findings support the hypothesis that the cerebellum is involved in the encoding and/or processing of prediction errors. The present findings are supported by earlier findings (Ploghaus et al., 2000) reporting activations of the posterolateral cerebellar hemisphere in the very first extinction trial in an associative learning task using painful heat stimuli as US. Our findings are also very similar to findings in a recent fMRI study on the cerebellar contributions to language (Moberget et al., 2014): Activation of the posterolateral cerebellum (Crus I and II) was related to the predictability of upcoming words in a sentence (e.g., two plus two is *four*). Similar to the present findings, prominent cerebellar activation was also observed when this prediction was violated (e.g., two plus two is *apple*). In the sensorimotor domain, fMRI data in humans also show cerebellar activation related to the unexpected omission of an expected sensory stimulus (Ramnani et al., 2000; Schlerf et al., 2012).

Based on theoretical models it has long been assumed that error information is sent to the cerebellar cortex via the climbing fibers (Albus, 1971; Marr, 1969). Climbing fibers have been shown to signal the unexpected occurrence and the unexpected omission of the airpuff-US in eyeblink conditioning in mice and rabbits (see Ohmae and Medina, 2015, for a recent study): Whereas the unexpected occurrence leads to an increase of climbing fiber activity, the unexpected omission results in a decrease. Because the fMRI signal is thought to reflect synaptic activity (Lauritzen et al., 2012), decrease of climbing fiber input cannot explain the observed increased fMRI signal in the cerebellar cortex during US omission. Prediction

errors, however, may not only be signaled by the climbing fiber system. There is also evidence that mossy fibers play a role (Popa et al., 2017; Streng et al., 2018). Furthermore, the role of the cerebellum may go beyond the processing of sensory predictions and sensory prediction errors and may include reward predictions and prediction errors (Carta et al., 2019; Wagner et al., 2017). Wagner et al. (2017) found granule cells that responded preferentially to reward, to reward omission and reward anticipation, a function commonly ascribed to the dopaminergic system (Schultz et al., 1997; Schultz, 2017). Importantly, reward omission granule cells were significantly more frequent than reward cells. In addition to sensory and reward prediction errors, the cerebellum may be involved in prediction of punishment and punishment prediction errors. As outlined in the introduction, several brain areas are likely involved in the processing of predictions and prediction errors in associative fear learning. As yet, it is unknown where prediction errors of learned fear responses are encoded (Tovote et al., 2015). Because there is some experimental evidence that sensory prediction errors are encoded in the cerebellar cortex and nuclei (Brooks et al., 2015; Ohmae and Medina, 2015; Popa and Ebner, 2018), the cerebellum is a likely candidate. However, this issue is far from being settled and extracerebellar areas may also play a role.

Changes in connectivity between the cerebellum and visual cortex

Functional connectivity of the cerebellum was increased with visual cortical areas when comparing CS+ with CS- trials and with limbic areas during presentation of the US, but not during its prediction. Likewise, Lithari et al. (2016) found that visual cortex processing plays a more central role and that limbic areas become functionally decoupled in a fear conditioning paradigm. Increased connectivity between the cerebellum and visual cortex suggests that the cerebellum contributes to the known enhancement of the perception of visual stimuli during fear conditioning (Petro et al., 2017).

However, at first sight, increased connectivity between the cerebellum and visual cortex is unexpected. In monkeys, the primary visual cortex has no known afferent connections with the cerebellum (Glickstein et al., 1994; Schmahmann and Pandya, 1997). Likewise, resting state fMRI revealed no functional connectivity between the cerebellum and primary visual cortex in a large study population (Buckner et al., 2011). Rather, the cerebellum receives dense afferent connections from the dorsal stream of parietal lobe visual areas (Glickstein,

2000; Schmahmann and Pandya, 1997) and is known to increase visual perception of movements (e.g., Christensen et al., 2014; Handel et al., 2009). The influence of the cerebellum on the perception of fear-conditioned visual stimuli may be indirect: Enhanced processing of fear conditioned visual stimuli in the visual cortex has been shown to be under the control of cortical structures, in particular the middle frontal gyrus (MFG; Petro et al., 2017). Bidirectional cerebello-frontal connections are known for the frontal eye field and the dorsolateral prefrontal cortex, which play an important role in attention (Middleton and Strick, 2001). Possibly, the cerebellum may help to increase selective attention to the CS.

Conclusions

The most important present finding is the pronounced cerebellar activation during the unexpected omission of a predicted aversive stimulus. This cerebellar activation is best explained by the generation or further processing of prediction errors. As expected, cerebellar activation was also found during the prediction of aversive stimuli. These findings support the hypothesis that the cerebellum is of general importance for predictive control including the emotional domain. The cerebellum has to be added to the more extended neural network involved in processing of aversive predictions and prediction errors.

Acknowledgments

The authors like to thank M. Craske for her valuable advice and fruitful discussions, J. Marquez for his support using the MP2RAGE sequence, B. Poser for his work on the SMS-EPI sequence, T. Otto for his work on SCR analysis, and B. Brol for work on the cerebellar masks. This work was supported by a grant from the German Research Foundation (DFG; project number 316803389 – SFB 1280) to D.T. and H.H.Q. (subproject A05), C.J.M. (subproject A09), and U.B. (subproject A11).

780 **References**

781 Albus, J.S., 1971. A theory of cerebellar function. Mathematical Biosciences. 10**,** 25-61.

782 Apps, R., Strata, P., 2015. Neuronal circuits for fear and anxiety - the missing link. Nat Rev
783 Neurosci. 16**,** 642.

784 Apps, R., et al., 2018. Cerebellar modules and their role as operational cerebellar processing
785 units. Cerebellum. Epub ahead of print.

786 Atlas, L.Y., et al., 2016. Instructed knowledge shapes feedback-driven aversive learning in
787 striatum and orbitofrontal cortex, but not the amygdala. Elife. 5**,** e15192.

788 Badura, A., et al., 2018. Normal cognitive and social development require posterior
789 cerebellar activity. Elife. 7.

790 Bastian, A.J., 2006. Learning to predict the future: the cerebellum adapts feedforward
791 movement control. Curr Opin Neurobiol. 16**,** 645-9.

792 Bazin, P.L., et al., 2014. A computational framework for ultra-high resolution cortical
793 segmentation at 7 Tesla. Neuroimage. 93**,** 201-9.

794 Blatt, G.J., Oblak, A.L., Schmahmann, J.D., 2013. Cerebellar connections with limbic circuits:
795 anatomy and functional implications. In: Handbook of the Cerebellum and Cerebellar
796 Disorders. Vol., M. Manto, J.D. Schmahmann, F. Rossi, D.L. Gruol, N. Koibuchi, eds.
797 Springer Netherlands, Dordrecht, pp. 479-96.

798 Blechert, J., et al., 2008. When two paradigms meet: Does evaluative learning extinguish in
799 differential fear conditioning? Learning and Motivation. 39**,** 58-70.

800 Boll, S., et al., 2013. Separate amygdala subregions signal surprise and predictiveness during
801 associative fear learning in humans. Eur J Neurosci. 37**,** 758-67.

802 Boucsein, W., 2012. Electrodermal activity, Vol., Springer, New York.

803 Brooks, J.X., Carriot, J., Cullen, K.E., 2015. Learning to expect the unexpected: rapid updating
804 in primate cerebellum during voluntary self-motion. Nat Neurosci. 18**,** 1310-7.

805 Buckner, R.L., et al., 2011. The organization of the human cerebellum estimated by intrinsic
806 functional connectivity. J Neurophysiol. 106**,** 2322-45.

807 Caligiore, D., et al., 2017. Consensus paper: towards a systems-level view of cerebellar
808 function: the interplay between cerebellum, basal ganglia, and cortex. Cerebellum.
809 16**,** 203-29.

810 Carta, I., et al., 2019. Cerebellar modulation of the reward circuitry and social behavior.
811 Science. 363**,** eaav0581.

812 Cauley, S.F., et al., 2014. Interslice leakage artifact reduction technique for simultaneous
813 multislice acquisitions. Magn Reson Med. 72**,** 93-102.

814 Christensen, A., et al., 2014. An intact action-perception coupling depends on the integrity of
815 the cerebellum. J Neurosci. 34**,** 6707-16.

816 Cui, S.Z., et al., 2000. Both sides of human cerebellum involved in preparation and execution
817 of sequential movements. Neuroreport. 11**,** 3849-53.

818 Diedrichsen, J., 2006. A spatially unbiased atlas template of the human cerebellum.
819 Neuroimage. 33**,** 127-38.

820 Diedrichsen, J., Zotow, E., 2015. Surface-based display of volume-averaged cerebellar
821 imaging data. PLoS One. 10**,** e0133402.

822 Dimitrova, A., et al., 2003. Cerebellar responses evoked by nociceptive leg withdrawal reflex
823 as revealed by event-related fMRI. J Neurophysiol. 90**,** 1877-86.

824 Ernst, T.M., et al., 2017. Modulation of 7 T fMRI signal in the cerebellar cortex and nuclei
825 during acquisition, extinction, and reacquisition of conditioned eyeblink responses.
826 Hum Brain Mapp. 38**,** 3957-74.

827 Fischer, H., et al., 2000. Fear conditioning and brain activity: a positron emission tomography
828 study in humans. Behav Neurosci. 114**,** 671-80.

829 Frings, M., et al., 2002. Involvement of the human cerebellum in fear-conditioned
830 potentiation of the acoustic startle response: a PET study. Neuroreport. 13**,** 1275-8.

831 Friston, K.J., et al., 1997. Psychophysiological and modulatory interactions in neuroimaging.
832 Neuroimage. 6**,** 218-29.

833 Frot, M., Faillenot, I., Mauguiere, F., 2014. Processing of nociceptive input from posterior to
834 anterior insula in humans. Hum Brain Mapp. 35**,** 5486-99.

835 Gallichan, D., Marques, J.P., 2017. Optimizing the acceleration and resolution of three-
836 dimensional fat image navigators for high-resolution motion correction at 7T. Magn
837 Reson Med. 77**,** 547-58.

838 Geuter, S., et al., 2017. Functional dissociation of stimulus intensity encoding and predictive
839 coding of pain in the insula. Elife. 6**,** e24770.

840 Glickstein, M., et al., 1994. Visual pontocerebellar projections in the macaque. J Comp
841 Neurol. 349**,** 51-72.

842 Glickstein, M., 2000. How are visual areas of the brain connected to motor areas for the
843 sensory guidance of movement? Trends Neurosci. 23**,** 613-7.

844 Glover, G.H., Li, T.Q., Ress, D., 2000. Image-based method for retrospective correction of
845 physiological motion effects in fMRI: RETROICOR. Magn Reson Med. 44**,** 162-7.

846 Handel, B., Thier, P., Haarmeier, T., 2009. Visual motion perception deficits due to cerebellar
847 lesions are paralleled by specific changes in cerebro-cortical activity. J Neurosci. 29**,**
848 15126-33.

849 Holland, P.C., Schiffino, F.L., 2016. Mini-review: Prediction errors, attention and associative
850 learning. Neurobiol Learn Mem. 131**,** 207-15.

851 Holmes, G., 1908. A form of familial degeneration of the cerebellum. Brain. 30**,** 466-89.

852 James, W., 1892. Text-book of Psychology, Vol., Macmillan, London.

853 King, M., et al., 2018. A multi-domain task battery reveals functional boundaries in the
854 human cerebellum. bioRxiv.

855 Lange, I., et al., 2015. The anatomy of fear learning in the cerebellum: a systematic meta-
856 analysis. Neurosci Biobehav Rev. 59**,** 83-91.

857 Lauritzen, M., et al., 2012. Neuronal inhibition and excitation, and the dichotomic control of
858 brain hemodynamic and oxygen responses. Neuroimage. 62**,** 1040-50.

859 Lesage, E., et al., 2012. Cerebellar rTMS disrupts predictive language processing. Curr Biol.
860 22**,** R794-R5.

861 Lesage, E., Hansen, P.C., Miall, R.C., 2017. Right lateral cerebellum represents linguistic
862 predictability. J Neurosci. 37**,** 6231-41.

863 Li, J., et al., 2011. Differential roles of human striatum and amygdala in associative learning.
864 Nat Neurosci. 14**,** 1250-2.

865 Li, S.S., McNally, G.P., 2014. The conditions that promote fear learning: prediction error and
866 Pavlovian fear conditioning. Neurobiol Learn Mem. 108**,** 14-21.

867 Lithari, C., Moratti, S., Weisz, N., 2016. Limbic areas are functionally decoupled and visual
868 cortex takes a more central role during fear conditioning in humans. Sci Rep. 6**,**
869 29220.

870 Marques, J.P., et al., 2010. MP2RAGE, a self bias-field corrected sequence for improved
871 segmentation and T1-mapping at high field. Neuroimage. 49**,** 1271-81.

872 Marr, D., 1969. A theory of cerebellar cortex. J Physiol. 202**,** 437-70.

873 Maschke, M., et al., 2002. Fear conditioned changes of heart rate in patients with medial
874 cerebellar lesions. J Neurol Neurosurg Psychiatry. 72**,** 116-8.

875 Maschke, M., et al., 2003. Cerebellar representation of the eyeblink response as revealed by
876 PET. Neuroreport. 14**,** 1371-4.

877 McCormick, D.A., Thompson, R.F., 1984. Cerebellum: essential involvement in the classically
878 conditioned eyelid response. Science. 223**,** 296-9.

879 Miall, R.C., et al., 1993. Is the cerebellum a smith predictor? J Mot Behav. 25**,** 203-16.

880 Miall, R.C., Galea, J., 2016. Cerebellar damage limits reinforcement learning. Brain. 139**,** 4-7.

881 Middleton, F.A., Strick, P.L., 1994. Anatomical evidence for cerebellar and basal ganglia
882 involvement in higher cognitive function. Science. 266**,** 458-61.

883 Middleton, F.A., Strick, P.L., 2000. Basal ganglia and cerebellar loops: motor and cognitive
884 circuits. Brain Res Brain Res Rev. 31**,** 236-50.

885 Middleton, F.A., Strick, P.L., 2001. Cerebellar projections to the prefrontal cortex of the
886 primate. J Neurosci. 21**,** 700-12.

887 Moberget, T., et al., 2014. Generalized role for the cerebellum in encoding internal models:
888 evidence from semantic processing. J Neurosci. 34**,** 2871-8.

889 Moulton, E.A., et al., 2010. The cerebellum and pain: passive integrator or active
890 participator? Brain Res Rev. 65**,** 14-27.

Mumford, J.A., 2012. A power calculation guide for fMRI studies. Soc Cogn Affect Neurosci. 7, 738-42.

Ohmae, S., Medina, J.F., 2015. Climbing fibers encode a temporal-difference prediction error during cerebellar learning in mice. Nat Neurosci. 18, 1798-803.

Oldfield, R.C., 1971. The assessment and analysis of handedness: the Edinburgh inventory. Neuropsychologia. 9, 97-113.

Petro, N.M., et al., 2017. Multimodal imaging evidence for a frontoparietal modulation of visual cortex during the selective processing of conditioned threat. J Cogn Neurosci. 29, 953-67.

Ploghaus, A., et al., 1999. Dissociating pain from its anticipation in the human brain. Science. 284, 1979-81.

Ploghaus, A., et al., 2000. Learning about pain: the neural substrate of the prediction error for aversive events. Proc Natl Acad Sci U S A. 97, 9281-6.

Popa, L.S., Hewitt, A.L., Ebner, T.J., 2012. Predictive and feedback performance errors are signaled in the simple spike discharge of individual Purkinje cells. J Neurosci. 32, 15345-58.

Popa, L.S., Hewitt, A.L., Ebner, T.J., 2014. The cerebellum for jocks and nerds alike. Front Syst Neurosci. 8, 113.

Popa, L.S., Streng, M.L., Ebner, T.J., 2017. Long-term predictive and feedback encoding of motor signals in the simple spike discharge of Purkinje cells. eNeuro. 4, ENEURO.0036-17.2017.

Popa, L.S., Ebner, T.J., 2018. Cerebellum, predictions and errors. Front Cell Neurosci. 12, 524.

Price, C.J., Friston, K.J., 1997. Cognitive conjunction: a new approach to brain activation experiments. NeuroImage. 5, 261-70.

Prokasy, W.F., Ebel, H.C., 1967. Three components of the classically conditioned GSR in human subjects. Journal of Experimental Psychology. 73, 247-56.

Ramnani, N., et al., 2000. Learning- and expectation-related changes in the human brain during motor learning. J Neurophysiol. 84, 3026-35.

Rescorla, R.A., Wagner, A.R., 1972. A theory of Pavlovian conditioning: variations in the effectiveness of reinforcement and nonreinforcement. In: Classical conditioning II: Current research and theory. Vol. 2, A.H. Black, W.F. Prokasy, eds. Appleton-Century-Crofts, New York, pp. 64-99.

Rorden, C., Brett, M., 2000. Stereotaxic display of brain lesions. Behav Neurol. 12**,** 191-200.

Sacchetti, B., et al., 2002. Cerebellar role in fear-conditioning consolidation. Proc Natl Acad Sci U S A. 99**,** 8406-11.

Schlerf, J.E., et al., 2010. Evidence of a novel somatopic map in the human neocerebellum during complex actions. J Neurophysiol. 103**,** 3330-6.

Schlerf, J.E., Ivry, R.B., Diedrichsen, J., 2012. Encoding of sensory prediction errors in the human cerebellum. J Neurosci. 32**,** 4913-22.

Schmahmann, J.D., Pandya, D.N., 1997. Anatomic organization of the basilar pontine projections from prefrontal cortices in rhesus monkey. J Neurosci. 17**,** 438-58.

Schmahmann, J.D., Sherman, J.C., 1998. The cerebellar cognitive affective syndrome. Brain. 121**,** 561-79.

Schmidt, K., et al., 2016. The differential effect of trigeminal vs. peripheral pain stimulation on visual processing and memory encoding is influenced by pain-related fear. Neuroimage. 134**,** 386-95.

Schultz, W., Dayan, P., Montague, P.R., 1997. A neural substrate of prediction and reward. Science. 275**,** 1593-9.

Schultz, W., 2017. Reward prediction error. Curr Biol. 27**,** R369-R71.

Setsompop, K., et al., 2012. Blipped-controlled aliasing in parallel imaging for simultaneous multislice echo planar imaging with reduced g-factor penalty. Magn Reson Med. 67**,** 1210-24.

Sokolov, A.A., Miall, R.C., Ivry, R.B., 2017. The cerebellum: adaptive prediction for movement and cognition. Trends Cogn Sci. 21**,** 313-32.

Stoodley, C.J., Schmahmann, J.D., 2018. Functional topography of the human cerebellum. Handb Clin Neurol. 154**,** 59-70.

947 Streng, M.L., Popa, L.S., Ebner, T.J., 2017a. Climbing fibers control Purkinje cell
948 representations of behavior. J Neurosci. 37**,** 1997-2009.

949 Streng, M.L., Popa, L.S., Ebner, T.J., 2017b. Climbing fibers predict movement kinematics and
950 performance errors. J Neurophysiol. 118**,** 1888-902.

951 Streng, M.L., Popa, L.S., Ebner, T.J., 2018. Modulation of sensory prediction error in Purkinje
952 cells during visual feedback manipulations. Nat Commun. 9**,** 1099.

953 Supple, W.F., Jr., Leaton, R.N., 1990. Lesions of the cerebellar vermis and cerebellar
954 hemispheres: effects on heart rate conditioning in rats. Behav Neurosci. 104**,** 934-47.

955 Supple, W.F., Jr., Kapp, B.S., 1993. The anterior cerebellar vermis: essential involvement in
956 classically conditioned bradycardia in the rabbit. J Neurosci. 13**,** 3705-11.

957 Tabbert, K., et al., 2011. Influence of contingency awareness on neural, electrodermal and
958 evaluative responses during fear conditioning. Soc Cogn Affect Neurosci. 6**,** 495-506.

959 Taylor, J.A., Ivry, R.B., 2014. Cerebellar and prefrontal cortex contributions to adaptation,
960 strategies, and reinforcement learning. Prog Brain Res. 210**,** 217-53.

961 Teeuwisse, W.M., Brink, W.M., Webb, A.G., 2012. Quantitative assessment of the effects of
962 high-permittivity pads in 7 Tesla MRI of the brain. Magn Reson Med. 67**,** 1285-93.

963 Thürling, M., et al., 2015. Cerebellar cortex and cerebellar nuclei are concomitantly activated
964 during eyeblink conditioning: a 7T fMRI study in humans. J Neurosci. 35**,** 1228-39.

965 Tovote, P., Fadok, J.P., Luthi, A., 2015. Neuronal circuits for fear and anxiety. Nat Rev
966 Neurosci. 16**,** 317-31.

967 Tzourio-Mazoyer, N., et al., 2002. Automated anatomical labeling of activations in SPM using
968 a macroscopic anatomical parcellation of the MNI MRI single-subject brain.
969 Neuroimage. 15**,** 273-89.

970 Vansteenwegen, D., et al., 2006. Resistance to extinction in evaluative conditioning. J Exp
971 Psychol Anim Behav Process. 32**,** 71-9.

972 Venables, P.H., Christie, M.J., 1980. Electrodermal activity. In: Techniques in
973 psychophysiology. Vol. 54, I. Martin, P.H. Venables, eds. Wiley, New York, pp. 3-67.

974 Verstynen, T.D., Deshpande, V., 2011. Using pulse oximetry to account for high and low
975 frequency physiological artifacts in the BOLD signal. Neuroimage. 55**,** 1633-44.

976 Vogt, B.A., 2014. Submodalities of emotion in the context of cingulate subregions. Cortex.
977 59, 197-202.

978 Wagner, M.J., et al., 2017. Cerebellar granule cells encode the expectation of reward.
979 Nature. 544, 96-100.

980 Welman, F.H.S.M., et al., 2018. Pain experience is somatotopically organized and overlaps
981 with pain anticipation in the human cerebellum. Cerebellum. 17, 447-60.

982 Wolpert, D.M., Miall, R.C., Kawato, M., 1998. Internal models in the cerebellum. Trends Cogn
983 Sci. 2, 338-47.

984

Supplementary Materials

Table of Content

Supplementary Figure 1: First interval skin conductance responses

Group mean first interval response (FIR). Error bars represent standard errors of the mean. hab = habituation, acq 1, acq 2 = early and late acquisition, ext 1, ext 2 = early and late extinction.

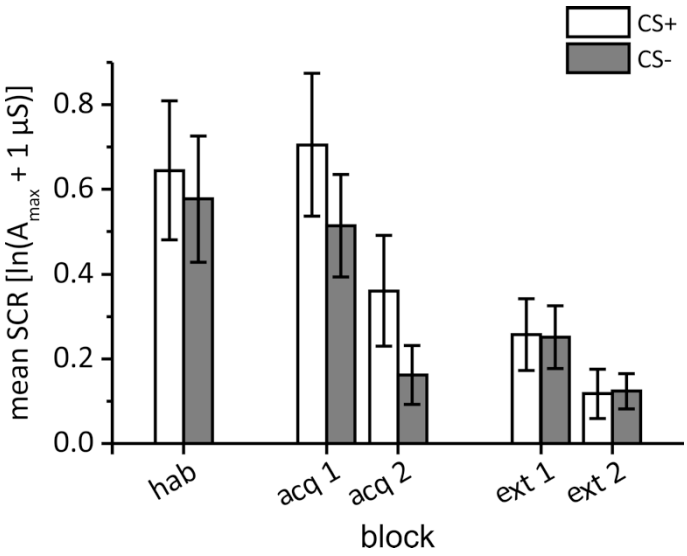

Supplementary Table 1: First interval skin conductance responses (Statistics)

Summary of statistical findings (repeated measures ANOVA; post-hoc *t*-tests). CS type = CS+ vs. CS-; phase = acquisition vs. extinction; block = early vs. late.

ANOVA	**contrast**	**degrees of freedom**	**F-value**	***P***
acquisition	CS type	1, 21	7.34	0.013
	block	1, 21	17.80	< 0.001
	CS type × block	1, 21	0.01	0.918
Extinction	CS type	1, 21	0.00	0.991
	block	1, 21	12.19	0.002
	CS type × block	1, 21	0.10	0.751
***t*-tests**	**contrast**	**degrees of freedom**	**t-value**	***p***
	Habituation, CS+ - CS-	21	1.12	0.275
	Early acquisition, CS+ - CS-	21	2.60	0.017
	Late acquisition, CS+ - CS-	21	2.22	0.038
	Early extinction, CS+ - CS-	21	0.15	0.882
	Late extinction, CS+ - CS-	21	-0.17	0.868

Supplementary Figure 2: Changes in cerebellar activation across blocks during acquisition and extinction

Changes in differential cerebellar activation across acquisition and extinction blocks based on F-tests **a)** related to the prediction of the US (contrast "CS+ > CS-"), and **b)** related to the omission of the US (contrast "no-US CS+ > no-US CS-") [$p < 0.05$ FWE corrected, using threshold-free cluster enhancement (TFCE); http://dbm.neuro.uni-jena.de/tfce/]. Mean β values across blocks are shown in the inserts. Note that all no-US CS+ trials were considered as a single block which was compared first against the early and then against the late "no-US post CS-" block. **c)** Cerebellar activation during extinction trials considering the contrast "no-US CS+ > no-US post CS-" ($p < 0.05$ FWE corrected, TFCE).

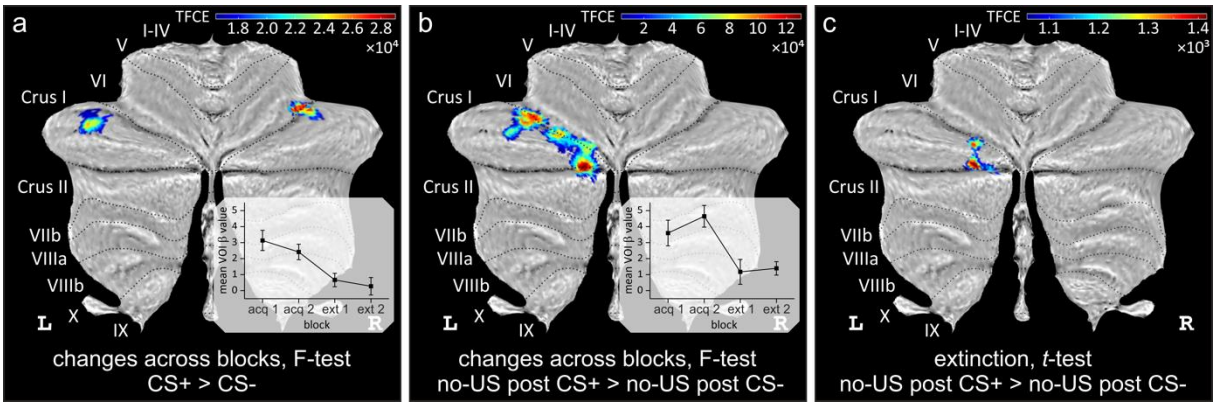

Supplementary Table 2: Changes in cerebellar activation across blocks during acquisition and extinction

Main effect of block during acquisition and extinction. Displayed are all clusters of 20 mm^3 or larger. In each cluster, up to three maxima are listed separated by 8 mm or more.

Index	Location (lobule)	Side	SUIT coordinates / mm			Cluster size / mm^3	p_{FWE}	TFCE
a) CS+ > CS- : Effect of block	***F-test, TFCE, p < 0.05 FWE corr.***							
1	VI	Right	35	-58	-28	294	0.004	28512.3
2	Extended cluster	left Crus I (239), left VI (1)						
	Crus I	Left	-43	-56	-32	240	0.006	24891.7
	Crus I	Left	-35	-52	-33		0.044	16501.8
b) no-US post CS+ > no-US post CS- : Effect of block	***F-test, TFCE, p < 0.05 FWE corr.***							
1	Extended cluster	left Crus I (776), left VI (311), left Crus II (118)						
	Crus I	Left	-12	-78	-32	1205	0.002	155108
	VI	Left	-27	-73	-25		0.002	137279
	VI	Left	-18	-75	-25		0.008	120878
2	Extended cluster	left Crus I (400), left VI (250)						
	VI	Left	-33	-64	-27	650	0.002	146662
	Crus I	Left	-35	-57	-31		0.002	137880
	Crus I	Left	-40	-64	-31		0.007	123883

Supplementary Figure 3: Comparison of cerebellar areas related to the presentation, the prediction and the omission of the aversive stimulus

(**a-c**) Common areas of cerebellar activation considering any two of the three main acquisition contrasts as revealed by conjunction analyses testing global null hypothesis; (**d-f**) significant differences in activation considering any two of the three main acquisition contrasts as revealed by F tests (using TFCE; inverse tests do not show any significant activation). All data presented at a significance level of $p < 0.05$ FWE-corrected.

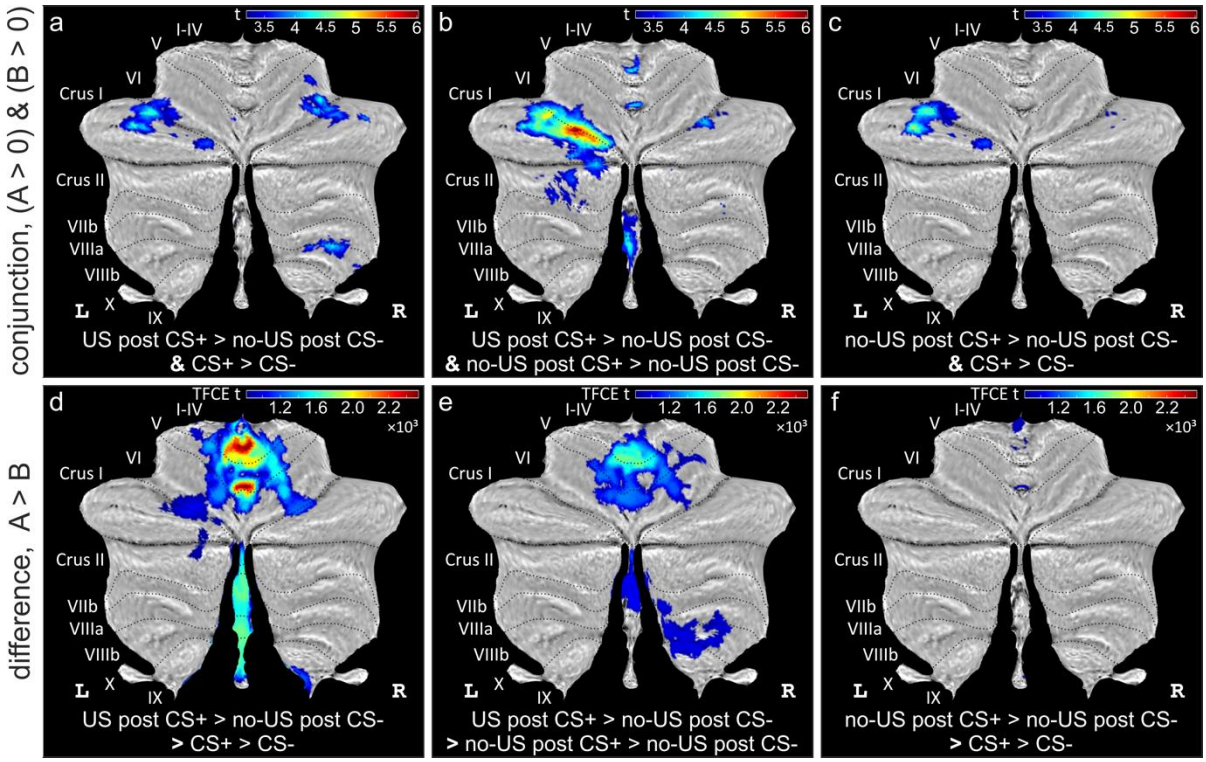

Supplementary Table 3: Cerebellar and whole brain conjunction analyses

Cerebellar regions identified using SUIT labels (Cerebellum-SUIT.nii, Diedrichsen, 2006); whole brain regions identified using AAL atlas labels (AAL.nii, Tzourio-Mazoyer et al., 2002). Clusters with 20 or more voxels are included (global null hypothesis, $p < 0.05$ FWE corrected). Up to three maxima per cluster are listed.

Index	Location	Side	SUIT coordinates / mm			Cluster size / mm^3	p_{FWE}	*t*
Cerebellar conjunction analysis: US post CS+ > no-US post CS- & CS+ > CS- & no-US post CS+ > no-US post CS- global null hypothesis, FWE corrected p < 0.05								
1	Extended cluster	left Crus I (2891), left VI (1715), left Crus II (108), gray matter (27)						
	Crus I	left	-32	-58	-34	4730	< 0.001	4.53
	Crus I	left	-44	-64	-29		< 0.001	4.45
	Crus I	left	-17	-77	-27		< 0.001	3.88
2	Extended cluster	right Crus I (697), right VI (409)						
	Crus I	right	39	-67	-28	1106	< 0.001	3.26
	Crus I	right	48	-61	-28		0.001	2.9
	VI	right	30	-69	-24		0.002	2.89
3	VIIIb	right	25	-56	-46	40	0.001	2.98
4	Crus II	left	-33	-62	-46	121	0.001	2.94
5	gray matter	left	-31	-53	-45	29	0.003	2.82
6	VIIb	right	32	-58	-46	27	0.003	2.79
Whole brain conjunction analysis: US post CS+ > no-US post CS- & CS+ > CS- & no-US post CS+ > no-US post CS- global null hypothesis, FWE corrected p < 0.05								
1	Extended cluster	left Insula (1916), left Frontal_Inf_Tri (790), left Frontal_Inf_Oper (738), left Frontal_Inf_Orb (221), outside GM (97), left Rolandic_Oper (64), left Temporal_Pole_Sup (15)						
	Insula	left	-31	17	4	3841	< 0.001	5.7
	Frontal_Inf_Tri	left	-42	15	7		< 0.001	4.6
	Insula	left	-31	26	-2		< 0.001	4.5
2	Extended cluster	right Insula (1770), right Frontal_Inf_Tri (973), right Frontal_Inf_Oper (905), outside GM (802), right Rolandic_Oper (140), right Frontal_Inf_Orb (112), right Putamen (73)						
	Frontal_Inf_Tri	right	37	27	2	4775	< 0.001	4.8
	Frontal_Inf_Oper	right	43	18	5		< 0.001	4.7
	Rolandic_Oper	right	53	6	8		< 0.001	3.9
3	Extended cluster	left Lob. Crus I (1839), left Lob. VI (1105), left Fusiform (1)						
	Lob. Crus I	left	-32	-59	-34	2945	< 0.001	4.7
	Lob. Crus I	left	-44	-66	-28		< 0.001	4.5
	Lob. Crus I	left	-18	-77	-27		< 0.001	3.7
4	Extended cluster	right SupraMarginal (2280), right Temporal_Sup (337), right Parietal_Inf (74), right Angular (48)						

	SupraMarginal	right	53	-43	28	2703	< 0.001	4.3
	SupraMarginal	right	60	-39	29		< 0.001	4.2
	SupraMarginal	right	54	-41	37		< 0.001	4.1
5	Extended cluster	outside GM (310), right Thalamus (12)						
	outside GM	right	5	-30	-8	322	< 0.001	4.2
	outside GM	right	7	-29	-19		< 0.001	3.7
6	Thalamus	right	11	-7	6	260	< 0.001	4.1
7	Extended cluster	right Precentral (391), right Frontal_Mid (301)						
	Precentral	right	44	8	50	692	< 0.001	4
	Precentral	right	43	2	39		< 0.001	3.4
8	Extended cluster	outside GM (208), left Thalamus (14)						
	outside GM	left	-9	-24	-8	222	< 0.001	3.9
	outside GM	left	-3	-30	-13		< 0.001	3.8
	outside GM	left	-3	-26	-3		0.01	2.9
9	Extended cluster	right Supp_Motor_Area (685), left Supp_Motor_Area (396), outside GM (6)						
	Supp_Motor_Area	right	6	15	51	1087	< 0.001	3.8
	Supp_Motor_Area	left	1	17	57		< 0.001	3.8
	Supp_Motor_Area	right	4	12	67		< 0.001	3.5
10	Extended cluster	right Lob. VI (339), right Lob. Crus I (73)						
	Lob. VI	right	37	-61	-27	412	< 0.001	3.7
	Lob. VI	right	26	-64	-32		< 0.001	3.4
	Lob. VI	right	35	-69	-26		0.004	3.1
11	Thalamus	left	-12	-9	7	162	< 0.001	3.6
12	outside GM	left	-7	-16	-10	38	< 0.001	3.5
13	Extended cluster	left SupraMarginal (576), left Parietal_Inf (148), outside GM (58)						
	SupraMarginal	left	-62	-46	32	779	< 0.001	3.5
	SupraMarginal	left	-60	-41	24		< 0.001	3.5
	SupraMarginal	left	-53	-41	32		< 0.001	3.4
14	Frontal_Sup	right	28	45	21	88	< 0.001	3.4
15	Frontal_Sup	right	23	52	22	147	< 0.001	3.4
16	Precentral	left	-39	-2	54	68	< 0.001	3.4
17	Lob. Crus II	left	-15	-75	-36	31	0.001	3.3
18	Supp_Motor_Area	left	-10	5	66	64	0.001	3.3
19	Frontal_Sup_Medial	left	1	30	33	203	0.001	3.3

Supplementary Table 4: Differences in cerebellar and whole brain activation

Differences in cerebellar activations comparing the three main acquisition contrasts based on *F*-tests (using TFCE, $p < 0.05$ FWE corrected). Cerebellar regions identified using SUIT labels; whole brain regions using AAL atlas labels. Clusters with 20 or more voxels are included. Up to three maxima per cluster are displayed.

Index	Location	Side	SUIT coordinates / mm			Cluster size / mm^3	p_{FWE}	TFCE F
Differences in cerebellar activations: US post CS+ > no-US post CS- vs. CS+ > CS- vs. no-US post CS+ > no-US post CS-								
		TFCE, FWE corrected p < 0.05						
1	Extended cluster	left Crus I (1021), left VI (563)						
	VI	left	-26	-73	-25	1584	0.002	755254
	Crus I	left	-17	-78	-25		0.002	733766
	Crus I	left	-37	-63	-27		0.017	508636
2	I-IV	right	3	-54	-22	136	0.014	520535
Differences in whole brain activations: US post CS+ > no-US post CS- vs. CS+ > CS- vs. no-US post CS+ > no-US post CS-								
		TFCE, FWE corrected p < 0.05						
1	Extended cluster	left Insula (5691), outside GM (843), left Frontal_Inf_Oper (801), left Temporal_Sup (499), left Frontal_Inf_Tri (427), left Frontal_Inf_Orb (304), left Temporal_Pole_Sup (129), left Rolandic_Oper (109), left Putamen (70), left Precentral (52), left Heschl (24)						
	Insula	left	-39	-4	-4	8949	< 0.001	3886919
	Temporal_Sup	left	-39	-14	-7		< 0.001	2220965
	Insula	left	-31	17	3		< 0.001	1613525
2	Extended cluster	right Insula (5594), outside GM (2030), right Frontal_Inf_Oper (1670), right Frontal_Inf_Tri (632), right Rolandic_Oper (557), right Frontal_Inf_Orb (517), right Putamen (315), right Temporal_Pole_Sup (74), right Temporal_Sup (28)						
	outside GM		39	-3	-8	11417	< 0.001	2200812
	Insula	right	42	9	-6		< 0.001	2126720
	Insula	right	40	-10	-4		< 0.001	2095510
3	Extended cluster	right SupraMarginal (811), right Temporal_Sup (56), outside GM (11), right Rolandic_Oper (6)						
	SupraMarginal	right	63	-38	27	884	0.001	1294068
	SupraMarginal	right	56	-33	27		0.008	1024451
	SupraMarginal	right	62	-26	22		0.016	9025467
4	outside GM	left	-5	-29	-8	179	0.010	966886
5	Extended cluster	left Lob. Crus I (240), left Lob. VI (195)						
	Lob. VI	left	-27	-74	-23	435	0.015	904621
	Lob. Crus I	left	-19	-78	-24		0.017	881553
6	SupraMarginal	left	-55	-39	25	244	0.018	862433
7	outside GM	left	-61	-37	41	40	0.036	785741
8	SupraMarginal	left	-59	-24	17	55	0.038	776401
9	Postcentral	left	-57	-23	25	33	0.039	772784

10	SupraMarginal	right	64	-33	36	37	0.042	760703

Supplementary Table 5: Whole brain activations during acquisition and extinction.

Displayed are all clusters of 20 mm^3 or larger. In each cluster up to three maxima are listed separated by 8 mm or more.

Index	Location	Side	SUIT coordinates / mm			Cluster size / mm^3	p_{FWE}	TFCE
US post CS+ > no-US post CS-	***FWE corrected p < 0.05***							
1	Extended cluster	outside GM (80294), left Insula (12830), right Frontal_Mid (12274), right Insula (12057), right SupraMarginal (11987), left Lob. Crus I (10060), left Lob. VI (9432), right Frontal_Inf_Tri (8704), left Cingulum_Mid (8377), right Lob. VI (7744), left SupraMarginal (7569), right Rolandic_Oper (6804), right Cingulum_Mid (6651), right Temporal_Mid (6472), right Temporal_Sup (6419), right Frontal_Inf_Oper (6290), right Supp_Motor_Area (6280), left Parietal_Inf (6124), left Supp_Motor_Area (5999), right Putamen (5904), right Lob. VIII (5843), left Rolandic_Oper (5485), left Calcarine (5359), left Frontal_Inf_Oper (5036), left Temporal_Sup (4941), left Cingulum_Ant (4765), left Lob. VIII (4743), right Frontal_Inf_Orb (4713), left Lob. IV-V (4711), left Lob. Crus II (4613), vermal Lob. IV-V (4533), right Parietal_Inf (4373), left Thalamus (4352), left Precuneus (4172), right Caudate (3976), left Putamen (3966), right Calcarine (3872), right Frontal_Sup_Medial (3740), right Thalamus (3555), right Lob. IV-V (3534), right Cingulum_Ant (3524), left Postcentral (3294), right Frontal_Sup (3091), left Frontal_Inf_Tri (2837), right Lob. IX (2752), left Frontal_Sup_Medial (2619), left Lingual (2361), right Precuneus (2331), left Frontal_Sup (2166), right Lob. Crus I (2113), left Caudate (2106), vermal Lob. VI (1945), left Frontal_Inf_Orb (1856), right Precentral (1738), right Lingual (1552), right Temporal_Pole_Sup (1540), left Lob. IX (1502), vermal Lob. VIII (1445), left Precentral (1378), left Temporal_Pole_Sup (1349), left Lob. VIIb (1280), left Pallidum (1139), vermal Lob. IX (1040), left Temporal_Inf (981), right Postcentral (952), left Heschl (923), right Pallidum (875), right Hippocampus (839), left Paracentralobule (757), right Amygdala (726), left Hippocampus (704), vermal Lob. III (667), right Frontal_Mid_Orb (631), right Angular (554), right Heschl (489), left Amygdala (472), right Temporal_Inf (436), left Paracentralobule (362), left Cuneus (357), right Frontal_Sup_Orb (347), left Fusiform (324), right Fusiform (302), right Parietal_Sup (300), right Lob. Crus II (300), left Lob. III (277), vermal Lob. VII (268), right Lob. VIIb (241), right Olfactory (205), right Lob. III (180), vermal Lob. X (166), vermal Lob. 1_2 (146), left ParaHippocampal (144), left Olfactory (115), right ParaHippocampal (80), left Lob. X (72), right Lob. X (72), left Cingulum_Post (71), right Temporal_Pole_Mid (53), left Frontal_Mid (31), right Cingulum_Post (25), left Temporal_Mid (21), right Rectus (19), right Cuneus (16), left Parietal_Sup (14), left Frontal_Sup_Orb (12), left Occipital_Sup (1)						
	Insula	right	42	-3	-7	390038	< 0.001	18195.4
	Insula	left	-37	-10	-5		< 0.001	18164.9
	Insula	right	41	-11	-9		< 0.001	17925.9
2	Extended cluster	left Precuneus (833), left Parietal_Sup (92), left Cuneus (60), left Occipital_Sup (34)						
	Precuneus	left	-9	-74	42	1019	0.029	3199.4
	Cuneus	left	-3	-80	40		0.047	2779.1
3	Extended cluster	left Parietal_Sup (1146), left Postcentral (577), left Precuneus (50), outside GM (26)						
	Postcentral	left	-25	-43	67	1799	0.032	3118.3
	Parietal_Sup	left	-18	-49	69		0.033	3102.4

	Postcentral	left	-25	-37	73		0.044	2855.1
4	Extended cluster	left Frontal_Mid (2317), left Frontal_Inf_Tri (1775), left Frontal_Sup (235), outside GM (91)						
	Frontal_Inf_Tri	left	-46	42	4	4418	0.033	3102.1
	Frontal_Mid	left	-31	49	24		0.036	3003.0
	Frontal_Mid	left	-45	39	21		0.036	3002.0
5	outside GM		33	-36	18	52	0.037	2997.7
6	outside GM		12	-92	-14	34	0.037	2984.9
7	Extended cluster	left Temporal_Mid (741), outside GM (17)						
	Temporal_Mid	left	-56	-58	3	758	0.037	2981.6
	outside GM		-46	-53	2		0.040	2939.3
	Temporal_Mid	left	-48	-54	10		0.041	2908.4
8	Frontal_Mid	left	-35	43	1	53	0.049	2758.8

CS+ > CS- ***FWE corrected p < 0.05***

1	Extended cluster	left Supp_Motor_Area (3488), left Cingulum_Mid (2817), right Supp_Motor_Area (2769), right Cingulum_Mid (1757), left Cingulum_Ant (701), left Frontal_Sup_Medial (684), outside GM (554), right Frontal_Sup_Medial (228), right Cingulum_Ant (209), left Frontal_Sup (58), right Frontal_Sup (53), left Precentral (3)						
	Supp_Motor_Area	right	2	10	61	13321	0.013	3708.7
	Cingulum_Ant	left	1	27	29		0.013	3676.5
	Supp_Motor_Area	left	-3	11	54		0.014	3631.8
2	Extended cluster	right SupraMarginal (1153), right Temporal_Sup (5), right Angular (4)						
	SupraMarginal	right	61	-41	27	1162	0.016	3519.4
	SupraMarginal	right	53	-40	29		0.020	3343.3
	SupraMarginal	right	50	-40	37		0.039	2764.9
3	Extended cluster	left Insula (1674), left Frontal_Inf_Tri (565), left Frontal_Inf_Orb (155), left Frontal_Inf_Oper (144), outside GM (18)						
	Insula	left	-39	15	7	2556	0.018	3442.6
	Insula	left	-30	17	7		0.018	3418.6
	Insula	left	-29	27	-2		0.022	3240.4
4	Extended cluster	right Lob. VI (729), right Lob. Crus I (332)						
	Lob. VI	right	35	-48	-30	1061	0.022	3252.6
	Lob. VI	right	32	-60	-24		0.025	3113.8
	Lob. Crus I	right	39	-58	-32		0.028	3016.2
5	Extended cluster	right Insula (1464), right Frontal_Inf_Tri (899), outside GM (745), right Frontal_Inf_Oper (369), right Frontal_Inf_Orb (164), right Putamen (1)						
	Frontal_Inf_Tri	right	39	29	1	3642	0.023	3214.5
	Insula	right	34	22	13		0.023	3190.4
	Insula	right	30	27	3		0.024	3148.5
6	outside GM		-6	-29	-7	200	0.023	3210.8
7	outside GM		9	-4	6	280	0.024	3138.4
8	Extended cluster	outside GM (182)						
	outside GM		6	-28	-7	182	0.026	3062.1

	outside GM		9	-27	-18		0.049	2596.5
9	Extended cluster	left Lob. Crus I (480), left Lob. VI (116)						
	Lob. Crus I	left	-44	-59	-32	596	0.032	2915.4
	Lob. Crus I	left	-37	-54	-34		0.034	2887.5
	Lob. Crus I	left	-31	-60	-33		0.045	2655.9
10	Extended cluster	left SupraMarginal (226)						
	SupraMarginal	left	-54	-41	31	226	0.046	2636.7
	SupraMarginal	left	-61	-46	32		0.049	2573.9

Acquisition – no-US post CS+ > no-US post CS- FWE corrected p < 0.05

1	Extended cluster	right Frontal_Mid (11734), outside GM (8351), right Frontal_Inf_Oper (5575), right Frontal_Inf_Tri (5442), right Insula (4346), right Frontal_Inf_Orb (2531), right Putamen (2180), right Frontal_Sup (2001), right Precentral (952), right Thalamus (481), right Caudate (458), right Rolandic_Oper (390), right Frontal_Mid_Orb (327), right Pallidum (278), right Frontal_Sup_Orb (224), right Temporal_Pole_Sup (119), left Thalamus (57), right Olfactory (3)						
	Insula	right	36	20	0	45449	0.001	4926.3
	Frontal_Inf_Orb	right	33	24	-11		0.001	4895.6
	Frontal_Inf_Tri	right	50	20	4		0.001	4781.1
2	Extended cluster	left Lob. Crus I (6445), left Lob. VI (3064), left Lob. Crus II (773), outside GM (119), left Fusiform (14), left Lob. VIII (4)						
	Lob. Crus I	left	-24	-77	-26	10419	0.001	4685.0
	Lob. Crus I	left	-35	-75	-24		0.001	4649.6
	Lob. Crus I	left	-15	-79	-22		0.001	4634.5
3	Extended cluster	left Insula (2780), left Frontal_Inf_Oper (1231), left Frontal_Inf_Tri (841), outside GM (642), left Putamen (499), left Frontal_Inf_Orb (424), left Rolandic_Oper (104), left Temporal_Pole_Sup (47), left Precentral (31)						
	Insula	left	-31	18	3	6599	0.002	4254.5
	Insula	left	-30	22	-7		0.003	4117.3
	Putamen	left	-27	11	4		0.006	3672.0
4	Extended cluster	left Frontal_Sup_Medial (3900), right Supp_Motor_Area (2877), right Frontal_Sup_Medial (2070), left Supp_Motor_Area (1762), right Cingulum_Mid (592), outside GM (290), right Frontal_Sup (216), left Cingulum_Ant (115), right Cingulum_Ant (104), left Cingulum_Mid (95), left Frontal_Sup (57)						
	Frontal_Sup_Medial	left	-5	27	49	12078	0.006	3607.7
	Supp_Motor_Area	right	6	19	58		0.011	3225.5
	Supp_Motor_Area	left	0	24	55		0.012	3212.4
5	Extended cluster	left Parietal_Inf (465), outside GM (259), left SupraMarginal (83)						
	outside GM		-60	-46	41	807	0.018	2923.1
	outside GM		-63	-51	33		0.023	2819.0
	outside GM		-60	-40	47		0.038	2539.2
6	Lob. IV-V	vermal	1	-55	-22	139	0.030	2661.4
7	Extended cluster	right SupraMarginal (178), right Angular (173)						
	Angular	right	52	-50	26	351	0.038	2534.1
	SupraMarginal	right	60	-49	26		0.041	2482.2
8	Extended cluster	right SupraMarginal (484), right Parietal_Inf (290), outside GM (7)						

	SupraMarginal	right	60	-47	42	781	0.040	2507.7
	SupraMarginal	right	54	-43	38		0.041	2472.1
	SupraMarginal	right	62	-34	39		0.042	2461.7
9	outside GM		-4	-8	-7	4	0.041	2476.7
10	Cingulum_Ant	right	12	17	27	38	0.046	2431.0
11	SupraMarginal	right	65	-40	27	24	0.049	2384.4

References

Diedrichsen, J., 2006. A spatially unbiased atlas template of the human cerebellum. Neuroimage. 33**,** 127-38.

Tzourio-Mazoyer, N., et al., 2002. Automated anatomical labeling of activations in SPM using a macroscopic anatomical parcellation of the MNI MRI single-subject brain. Neuroimage. 15**,** 273-89.